

## EXPERIMENTAL, COMPUTATIONAL, AND OBSERVATIONAL ANALYSIS OF PRIMORDIAL NUCLEOSYNTHESIS

MICHAEL S. SMITH<sup>1</sup> AND LAWRENCE H. KAWANO

W. K. Kellogg Radiation Laboratory 106-38, California Institute of Technology, Pasadena, CA 91125

AND

ROBERT A. MALANEY

Canadian Institute for Theoretical Astrophysics, University of Toronto, Toronto, Canada M5S 1A7

Received 1992 May 22; accepted 1992 September 8

### ABSTRACT

We present a comprehensive evaluation of the current status of the standard theory of primordial nucleosynthesis. We determine the 12 nuclear reactions most important for the production of the light elements and conduct a detailed study of their rates and uncertainties, incorporating these into a Monte Carlo analysis to properly evaluate uncertainties in the computed elemental abundances. We then compare these predicted abundances with primordial abundances deduced from astronomical observations of the light elements D,  $^3\text{He}$ ,  $^4\text{He}$ , and  $^7\text{Li}$  and find a consistent agreement over a narrow range of the baryon-to-photon ratio  $\eta$ , thereby supporting the standard theory of big bang nucleosynthesis. This  $\eta$  range corresponds to a constraint on the baryon density parameter of  $0.01 \leq \Omega_b \leq 0.09$ , where the primordial D +  $^3\text{He}$  abundance sets the lower bound and the  $^4\text{He}$  abundance sets the upper bound. The new reaction rates cause an increase in the upper bound from  $^7\text{Li}$  by 40% over that determined in previous studies. With this new constraint on  $\Omega_b$ , observational evidence for  $Y_p < 0.237$  will require either a reinterpretation of the D +  $^3\text{He}$  bound or modifications to standard nucleosynthesis theory.

*Subject headings:* early universe — nuclear reactions, nucleosynthesis, abundances

### 1. INTRODUCTION

The current status of the standard primordial or big bang nucleosynthesis (SBBN) theory has been most recently reviewed by Krauss & Romanelli (1990) and by Walker et al. (1991). The work of Krauss & Romanelli is most notable for incorporating a Monte Carlo analysis into the abundance computations: their resulting 1  $\sigma$  and 2  $\sigma$  abundance curves allowed the full effect of reaction rate uncertainties on predicted abundances to be appreciated for the first time. Walker et al., while updating some of the reaction rates, concentrated primarily on the observational sector, doing a careful examination of the issues surrounding the extraction of limits on primordial abundances from current observations. Their analysis gave an upper bound on the baryon closure density of  $\Omega_b \leq 0.10$ .

These fine papers notwithstanding, we believe there is justification for undertaking another examination of the current SBBN model. The motivations for the present work are as follows:

1. *New reaction rates.*—The latest tabulation of reaction rates by Caughlan & Fowler (1988, hereafter CF88) was not available to Krauss and Romanelli for use in their Monte Carlo analysis. Although Walker et al. were able to make use of these new rates, there have since been new measurements of the neutron lifetime and of the important d(d, n) $^3\text{He}$ , d(d, p)t, t( $\alpha$ ,  $\gamma$ ) $^7\text{Li}$ ,  $^3\text{He}(\alpha, \gamma)^7\text{Be}$ , and  $^7\text{Li}(p, \alpha)^4\text{He}$  reactions. In our nucleosynthesis computations, we use neutron lifetime measurements dating no earlier than 1986.

2. *New theoretical developments in interpreting observational abundances.*—Some recent theoretical work (Deliannis & Pinsonneault 1993; Pinsonneault, Deliannis, & Demarque 1992) have suggested that rotational effects can allow for essentially uniform  $^7\text{Li}$  depletion in Population II stars, making less certain the claim that the  $^7\text{Li}$  abundances in these stars are primordial. Because of the importance of the  $^7\text{Li}$  abundance in putting an upper bound on the baryon-to-photon ratio  $\eta$ , this development calls into question previous upper limits on  $\Omega_b$ . There has also been recent work (Fuller, Boyd, & Kalen 1991) estimating a fairly low value for primordial  $^4\text{He}$ .

3. *Treatment from the perspective of nuclear physics.*—Previous reviews of the status of SBBN have generally been from the standpoint of cosmology, offering only limited insight into the nuclear physics aspects of the reaction measurements. In this study, we do an extensive review of experimental data on reactions crucially important to big bang light-element production. Using all available data, we determine the reaction rates with uncertainties appropriate for the temperature range of SBBN, presenting details of our analysis techniques. We also highlight the reactions most in need of further experimental and theoretical analysis.

4. *Treatment of computational errors.*—When computing abundances in SBBN, the main uncertainties arise from reaction rate uncertainties, which were given full attention for the first time in the Monte Carlo analysis of Krauss and Romanelli. We extend their analysis by incorporating temperature-dependent rate uncertainties and by increasing the number of reaction rates varied in the Monte Carlo analysis to 12. Additionally, we correct for errors that arise from the numerical computation itself (see Kawano 1992), which have been neglected in most SBBN studies. These errors, though relatively

<sup>1</sup> Postal Address: Physics Division, Oak Ridge National Laboratory, ms-6371, P.O. Box 2008, Oak Ridge, TN 37831-6371.

small, are not insignificant: for example, the nucleosynthesis code of Kawano (1988), used both by Krauss and Romanelli and Walker et al., has computational errors as large as 6% (for  $^7\text{Li}$  at low  $\eta$ -values).

*5. A desire for caution.*—It seems clear from previous studies of SBBN that the baryon density falls short of closing the universe; however, we are less confident of the specific upper limits on the baryon density given by previous studies. We are even less certain of reports that have already claimed the *inconsistency* of the standard SBBN model with observations (Riley & Irvine 1991). There are, as mentioned above, enough uncertainties in the observations to warrant a very cautious approach in setting observational limits. Furthermore, only a complete treatment of the reaction rates and numerical analysis can give confidence to the computational results. Our goal is to find the most reasonable limits to  $\Omega_b$  given all the known uncertainties.

*6. A desire for completeness and comprehensiveness.*—The Krauss and Romanelli work places emphasis on the reactions and the numerical analysis; the Walker et al. work has its strength in its evaluation of the observational data. We feel that both aspects need to be brought together in an up-to-date study to produce both a definitive picture of the current status of SBBN and a reliable constraint on the baryon density.

These motivating concerns and developments shaped the structure of our investigation: we have formulated a comprehensive experimental, computational, and observational analysis of SBBN with equal emphasis on the experimental reaction rate measurements from the laboratory and the empirical abundance constraints from the observatory. We proceed cautiously, using  $2\sigma$  uncertainty levels on the computed abundances and making very conservative determinations of observational constraints. Our approach, although conservative, reflects recent advances made in the field: we employ a mean neutron lifetime obtained from only the most recent experiments with a significant reduction in systematic uncertainties; and we evaluate our nucleosynthesis results in the standard model for three neutrino families in accordance with the results from measurements at CERN.

Our paper is structured in the following way: in § 2 we review salient features of SBBN physics and evaluate the relative contribution of the various nuclear reactions in order to determine those most important for light-element production. In § 3 we examine the experimental data on these primary reactions to obtain the best possible fits with uncertainties for these rates, and in § 4 we discuss the Monte Carlo analysis and the resulting computational abundances. In § 5 we discuss observational constraints on the elemental abundances, and in § 6 we compare these observational constraints with our computational results to put limits on the baryon density. We conclude with final remarks in § 7.

## 2. EVOLUTION OF ABUNDANCES AND PRIMARY REACTIONS

We begin with a review of primordial nucleosynthesis, focusing on the evolution of nuclide abundances. Other aspects such as neutrino decoupling and electron-positron annihilation can be found in the books of Weinberg (1972) and Kolb & Turner (1990).

### 2.1. The Neutron-Proton Ratio

At high temperatures ( $T \gg 0.8$  MeV), weak interactions are fast enough to keep neutrons and protons in statistical equilibrium. Initially, this means that neutrons and protons are in equal numbers. As the universe cools, the neutron-proton mass difference  $M_n - M_p = 1.293$  MeV ( $\equiv Q$ ) reduces the number of neutrons relative to protons via the relation

$$\left(\frac{n}{p}\right) = \exp(-Q/T). \quad (1)$$

When the universe has cooled to a temperature of about 0.8 MeV, the weak interaction rate—now comparable to the expansion rate—is no longer fast enough to keep neutrons and protons in equilibrium: the n/p ratio diverges from its equilibrium value (eq. [1]) and “freezes-out” (Fig. 1). The ratio does not, however, remain constant. Because neutron decay continues unabated, the n/p ratio continues to decrease, following the curve indicated in Figure 1. At a temperature of about 0.07 MeV, all the neutrons are processed into nuclei and the number of neutrons becomes constant thereafter.

The neutron lifetime  $\tau_n$ , which parameterizes the strength of the weak interactions, determines the temperature at which the n/p ratio freezes out and therefore the amount of  $^4\text{He}$  produced. Note that a larger  $\tau_n$  means that the weak interactions are weakened, resulting in a higher freeze-out temperature and (from eq. [1]) a higher n/p ratio. Because most of the neutrons get processed into  $^4\text{He}$ , a larger  $\tau_n$  results in an increase in the  $^4\text{He}$  abundance. In fact, the uncertainty in the neutron lifetime accounts for approximately 90% of the uncertainty in the predicted  $^4\text{He}$  abundance.

### 2.2. Light Elements in Nuclear Statistical Equilibrium

Figure 2 shows the evolution of the light-element abundances with decreasing temperature (note that the abundance of free neutrons is displayed); the value of the baryon-to-photon ratio

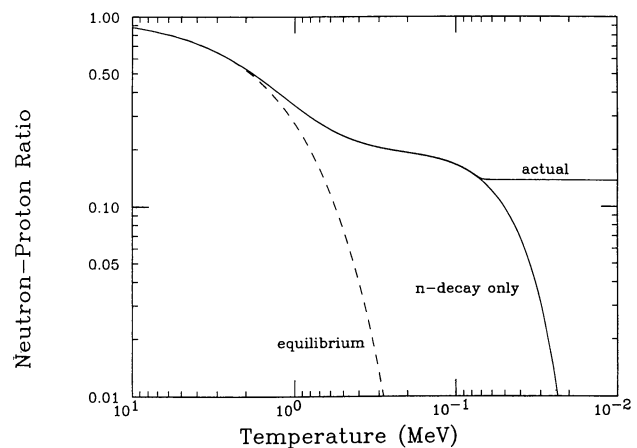


FIG. 1.—Evolution of the neutron-proton ratio with temperature. The NSE ratio is given by the dashed curve. If neutron decay is the only reaction (all other reactions are shut off), the n/p ratio follows the solid curve. The actual final value of the ratio is shown by the straight horizontal line.

ton ratio used is  $\eta = 10^{-9.5}$ , or  $\eta_{10} = 3.16$ , where  $\eta_{10} \equiv 10^{10}\eta$ . In this section, we focus on the evolution of the deuterium (d), tritium (t),  $^3\text{He}$ , and  $^4\text{He}$  nuclides, viewing nucleosynthesis as a series of departures from nuclear statistical equilibrium (NSE). There are four temperatures at which these departures occur: 0.8 MeV, as discussed above, when neutrons and protons cease interacting with one another; 0.6 MeV, when  $^4\text{He}$  leaves NSE; 0.2 MeV, when  $^3\text{He}$  and t stop interacting with d; and 0.07 MeV, when d finally falls out of equilibrium with n and p. There is also a departure at 0.08 MeV when t and  $^3\text{He}$  stop interacting with each other.

We will now discuss these series of events in greater detail. Above 0.6 MeV,  $^4\text{He}$  is in NSE with  $^3\text{He}$  and t,  $^3\text{He}$  is in NSE with t, both  $^3\text{He}$  and t are in equilibrium with d, and d is in equilibrium with n and p. Thus, their mass fractions,  $X_i$ , are given by their NSE values:

$$X_d = 16.3(T/m_n)^{3/2}\eta \exp(2.22/T)X_nX_p \quad (2)$$

$$X_t = 57.4(T/m_n)^3\eta^2 \exp(8.50/T)X_n^2X_p \quad (3)$$

$$X_3 = 57.4(T/m_n)^3\eta^2 \exp(7.72/T)X_nX_p^2 \quad (4)$$

$$X_4 = 113(T/m_n)^{9/2}\eta^3 \exp(28.3/T)X_n^2X_p^2. \quad (5)$$

In these expressions, the subscript 3 is for  $^3\text{He}$  and 4 for  $^4\text{He}$ ;  $m_n$  is the nucleon mass;  $T$  is the temperature in MeV; and the numbers in the exponents are the binding energies of the nuclides (in MeV). These NSE abundances are given in Figure 2 by the dashed lines. The dashed line for deuterium, plotted to correspond to the other NSE curves, assumes a constant neutron abundance; the actual deuterium NSE abundance is given by the dotted line.

In Figure 2, we see that the  $^4\text{He}$  abundance follows its NSE abundance curve for  $T > 0.6$  MeV. Were this to continue to lower temperatures,  $^4\text{He}$  would dominate all abundances by  $T = 0.3$  MeV (note that this is significantly lower than the 28

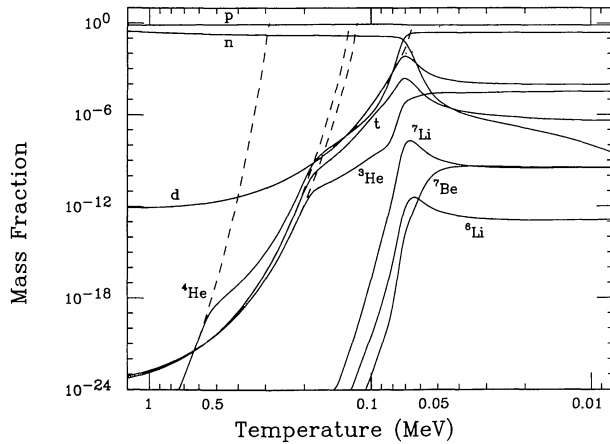


FIG. 2.—Evolution of light-element abundances with temperature, for a baryon-to-photon ratio  $\eta_{10} = 3.16$ . The dashed curves give the NSE curves of  $^4\text{He}$ , t,  $^3\text{He}$ , and d, respectively. The dotted curve is explained in the text.

MeV binding energy of  $^4\text{He}$ , due to the prefactors of the exponential in eq. [5]).  $^4\text{He}$  is, however, formed through  $^3\text{He}$  and t and is therefore in NSE only through these two nuclides. The  $^3\text{He}$  and t NSE abundances do not rise as fast as that for  $^4\text{He}$ , so when the mass-3 and mass-4 NSE curves cross at  $T \approx 0.6$  MeV,  $^4\text{He}$  is forced to leave its NSE track and plod along with these mass-3 nuclides. At  $T = 0.6$  MeV, the two reactions that keep  $^4\text{He}$  in equilibrium with  $^3\text{He}$  and t,  $^3\text{He}(n, \gamma)^4\text{He}$  and  $t(p, \gamma)^4\text{He}$ , are no longer fast enough relative to the expansion rate  $H$  to maintain the NSE abundance  $Y_{eq}$  (Fig. 3a). Because the  $^4\text{He}$  abundance falls off its NSE track, the reverse reactions slow down relative to those in the forward direction, as shown in Figure 3b. We therefore see that a short-lived but effective  $^3\text{He}$  and t bottleneck prevents  $^4\text{He}$  from dominating all the abundances immediately.  $^4\text{He}$  follows the mass-3 nuclides along their NSE curves until they too encounter a bottleneck at 0.2 MeV: the reactions  $d(n, \gamma)t$  and  $d(p, \gamma)^3\text{He}$ , which keep the mass-3 nuclides in equilibrium with d, slow down at this temperature, as shown in Figures 3a and 3b. The abundances of  $^3\text{He}$ , t, and  $^4\text{He}$  are limited by the formation of deuterium (a minor “deuterium bottleneck”), and follow along the deuterium NSE curve. Note that  $^3\text{He}$ , still in equilibrium with t via the  $^3\text{He}(n, p)t$  reaction, has its abundance suppressed relative to that of t until  $T = 0.08$  MeV when this reaction slows down. Finally, the deuterium abundance departs from its NSE track at about 0.07 MeV.

### 2.3. Light Elements in Quasi-Statistical Equilibrium

As the last of the light elements fall out of NSE,  $^4\text{He}$  production peaks and most of the neutrons are rapidly assimilated in  $^4\text{He}$ :  $X_4 \approx 2Y_n(\text{final})$ , where  $Y_i = X_i/A_i$ ,  $X_i$  is the mass fraction contained in nuclide  $i$ , and  $A_i$  is the mass number of nuclide  $i$ . Collisions of d, t, and  $^3\text{He}$  on the now abundant  $^4\text{He}$  begin producing  $^6\text{Li}$ ,  $^7\text{Li}$ , and  $^7\text{Be}$ . These heavier nuclides, as well as d, t, and  $^3\text{He}$ , are now in quasi-static equilibrium (QSE). Previously, the states of nuclear statistical equilibrium were maintained by reactions of equal magnitude in both forward and reverse directions (Fig. 3b). In quasi-static equilibrium, this is no longer the case; however, the total forward processing rate of all reactions is still essentially the same in magnitude as the total reverse processing rate. Given that the abundance of a nuclide  $i$  is governed by

$$\frac{dY_i}{dt} = \sum_{k,l} Y_k Y_l [kl] - \sum_j Y_i Y_j [ij], \quad (6)$$

with  $[ij]$  the rate for destroying  $i$  and  $[kl]$  the rate for creating  $i$ , the condition of QSE gives the temperature-dependent solution

$$Y_i(T) = \frac{\sum_{k,l} Y_k Y_l [kl]}{\sum_j Y_j [ij]}. \quad (7)$$

This is maintained as long as the reactions destroying  $i$  stay rapid relative to the expansion rate. As the temperature drops, the reactions which maintain QSE slow down relative to the expansion rate until the abundance freezes out at a tempera-

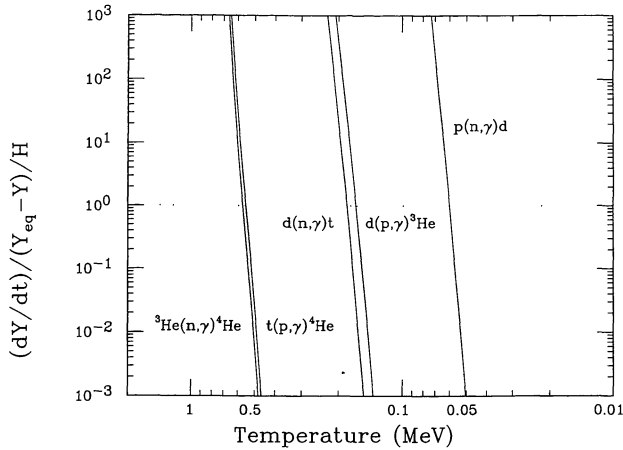


FIG. 3a

FIG. 3.—Illustration of the departure from NSE. (a) A measure of how fast reactions must be relative to the expansion rate in order to keep the elements at their NSE abundance  $Y_{eq}$ , for the five reactions that keep the light elements in NSE.  $dY/dT$  is the processing rate, and  $(Y - Y_{eq})/H$  is the difference between the actual and equilibrium abundance relative to the expansion rate  $H$ . (b) The ratio of the forward to reverse reaction rates for the same five reactions.

ture  $T_f$ :

$$Y_i(\text{final}) = \frac{\sum_{k,l} Y_k(T_f) Y_l(T_f) [kl](T_f)}{\sum_j Y_j(T_f) [ij](T_f)}. \quad (8)$$

For  $\eta_{10} = 3.16$ , the freeze-out temperatures are 0.03 MeV for d and  ${}^3\text{He}$ , 0.02 MeV for  ${}^7\text{Li}$  and  ${}^7\text{Be}$ , and 0.009 MeV for t. Esmailzadeh, Starkman, & Dimopoulos (1991) have analyzed the evolution of nucleosynthesis abundances through QSE solutions and freeze-out temperatures, and their discussion provides a detailed analytical account of an approximate determination of the final abundances of these elements.

#### 2.4. Determination of Important Nuclear Reactions

Having reviewed the temperature evolution of the light-element abundances, we will now evaluate the relative contributions of individual nuclear reactions to this process. Figures 4–9 show the main channels of creation and destruction of d, t,  ${}^3\text{He}$ ,  ${}^4\text{He}$ ,  ${}^7\text{Li}$ , and  ${}^7\text{Be}$ , for  $\eta_{10} = 3.16$ . For the creation of a nuclide  $i$  from nuclides  $k$  and  $l$ , we have displayed the processing rate  $Y_k Y_l [kl]$  divided by the expansion rate; for the destruction of the nuclide  $i$  in collision with a nuclide  $j$ , we plot the processing rate  $Y_i Y_j [ij]$  divided by the expansion rate. Although we have listed the reactions in order of their prominence during peak activity of nucleosynthesis, the final abundances of the nuclides, as discussed above, have a dependence on the rates of reactions at freeze-out. At different values of  $\eta$ , the qualitative features of these plots remain unchanged; however, there are some shifts of primacy among secondary reactions for  ${}^7\text{Be}$ .

There are a number of features to note in these figures. We see that the  $d(d, \gamma){}^4\text{He}$  reaction, previously suggested as being important in  ${}^4\text{He}$  production, is completely negligible. We also see that  ${}^4\text{He}$  is produced mainly through tritium via  $t(d, n){}^4\text{He}$  [as opposed to through  ${}^3\text{He}$  via  ${}^3\text{He}(d, p){}^4\text{He}$ ] and that tritium is created almost equally from  ${}^3\text{He}$  through  ${}^3\text{He}(n, p)t$  and from d through  $d(d, p)t$ . Our analysis leads us to the conclu-

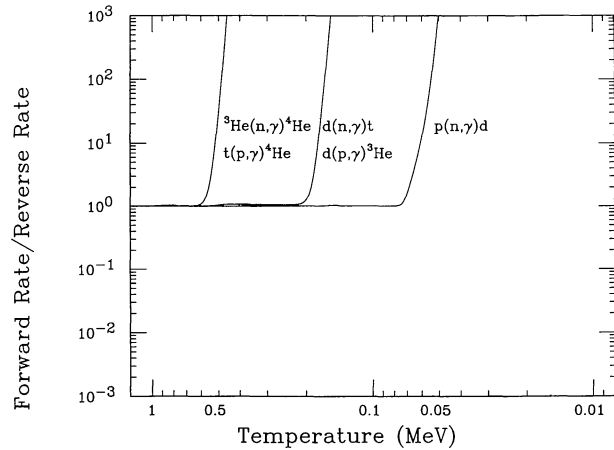


FIG. 3b

sion that there are 12 reactions, including neutron decay, of primary importance in the production of the light elements. These reactions are shown schematically in Figure 10. Krauss & Romanelli (1990) used 10 of these reactions, omitting  ${}^3\text{He}(n, p)t$  and  ${}^3\text{He}(d, p){}^4\text{He}$ ; Riley & Irvine (1991) did a variational study of reaction rates to see effects on the nuclide abundances and found these same 12 reactions to be the most important.

These 12 reactions form the basis of our experimental and computational analysis. In the next section, we will thoroughly examine the experimental data on these reactions to produce best-fit reaction rates and reaction uncertainties. We will subsequently use these rates and uncertainties in a Monte Carlo analysis of primordial nucleosynthesis abundances, described in § 4.

### 3. NUCLEAR REACTION RATES AND UNCERTAINTIES

#### 3.1. Introduction

The procedure for obtaining thermonuclear reaction rates from laboratory cross section measurements is discussed, for example, in Fowler, Caughlan, & Zimmerman (1967), Clayton (1983), and Rolfs & Rodney (1988). Rates for many astrophysically-important reactions are tabulated as analytic functions of temperature in the well-known compilations of Fowler et al. (1967, hereafter FCZI), Fowler et al. (1975, hereafter FCZII), Harris et al. (1983, hereafter HFCZ), and CF88. The first purpose of our study is to update these reaction rate compilations, incorporating new measurements of the neutron lifetime  $\tau_n$  and of the  $d(d, n){}^3\text{He}$ ,  $d(d, p)t$ ,  ${}^3\text{He}(\alpha, \gamma){}^7\text{Be}$ ,  $t(\alpha, \gamma){}^7\text{Li}$ , and  ${}^7\text{Li}(p, \alpha){}^4\text{He}$  reactions. The second purpose is to present a detailed description of the procedure to obtain thermonuclear reaction rates appropriate for the temperature range of SBBN from measurements of laboratory cross sections. As we discuss below, certain reaction rates in the compilations were formulated as stellar nucleosynthesis rates, appropriate at temperatures well below that of BBN. The evolution of light-

Processing Rate

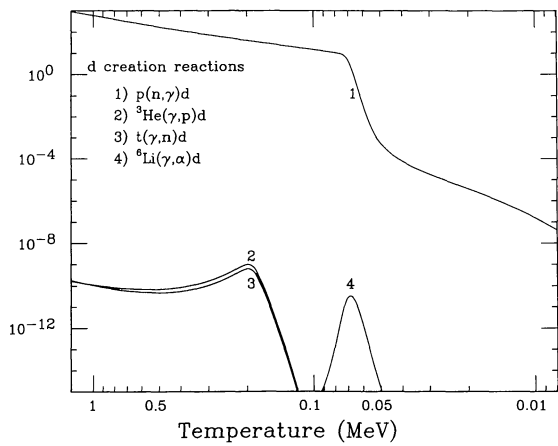


FIG. 4a

FIG. 4.—Processing rates of the most important reactions for the (a) creation and (b) destruction of deuterium

Processing Rate

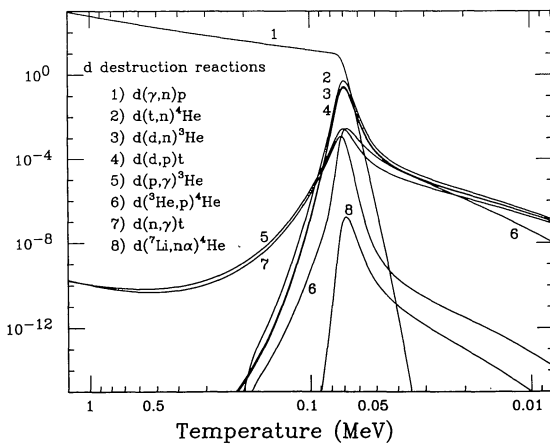


FIG. 4b

Processing Rate

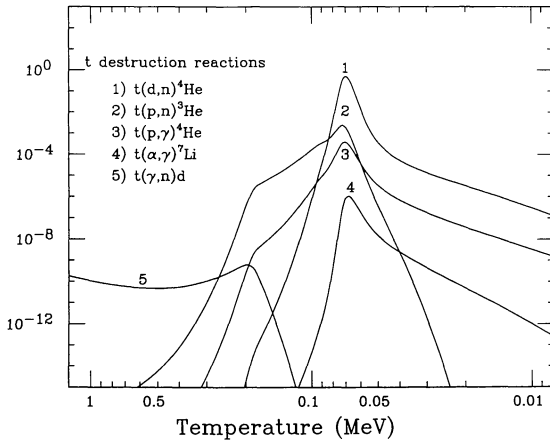


FIG. 5a

FIG. 5.—Processing rates of the most important reactions for the (a) creation and (b) destruction of tritium

Processing Rate

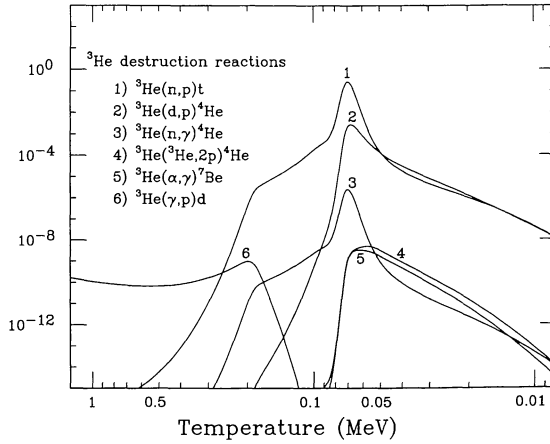


FIG. 5b

Processing Rate

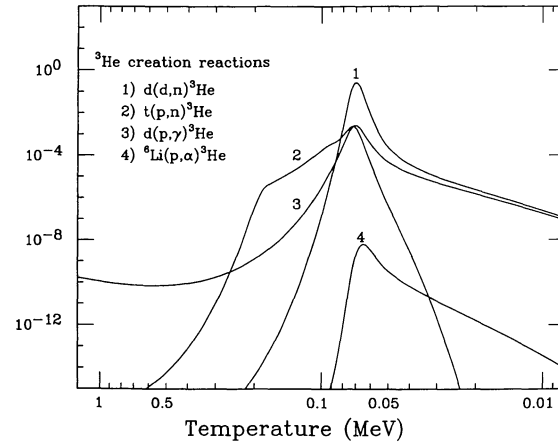


FIG. 6a

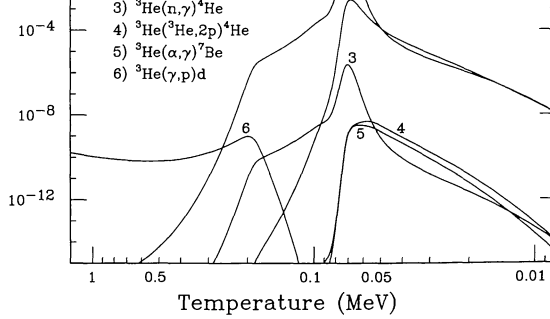
FIG. 6.—Processing rates of the most important reactions for the (a) creation and (b) destruction of  $^3\text{He}$ 

FIG. 6b

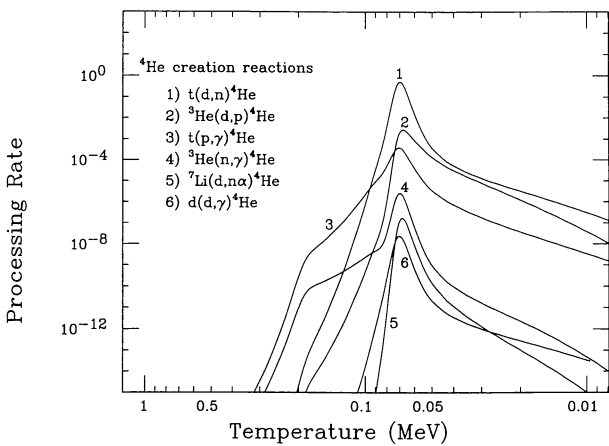


FIG. 7a

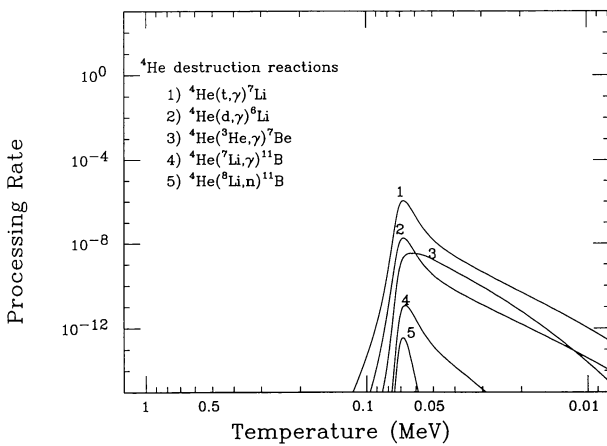
FIG. 7.—Processing rates of the most important reactions for the (a) creation and (b) destruction of  $^4\text{He}$ 

FIG. 7b

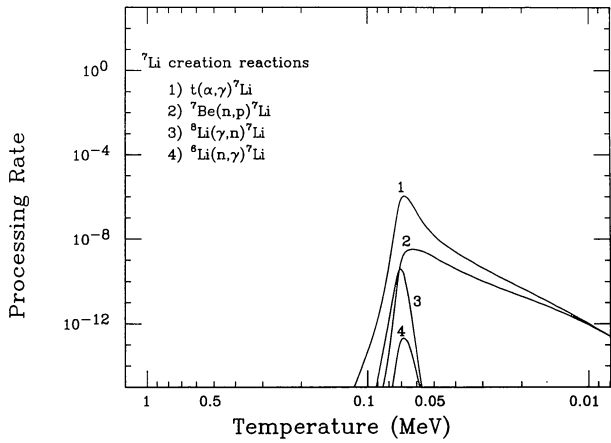


FIG. 8a

FIG. 8.—Processing rates of the most important reactions for the (a) creation and (b) destruction of lithium

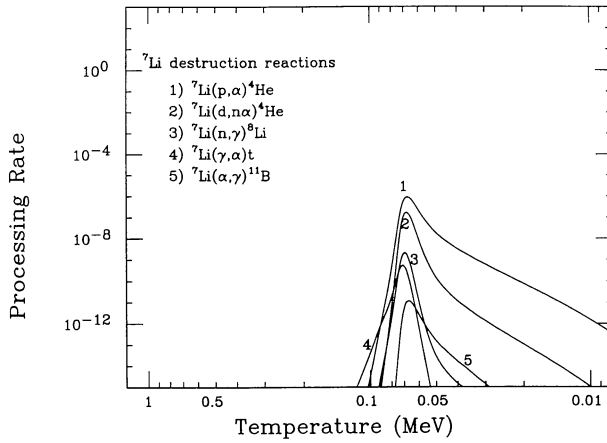


FIG. 8b

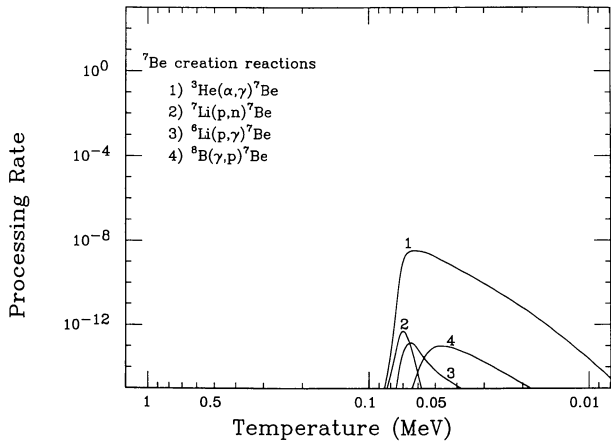


FIG. 9a

FIG. 9.—Processing rates of the most important reactions for the (a) creation and (b) destruction of beryllium

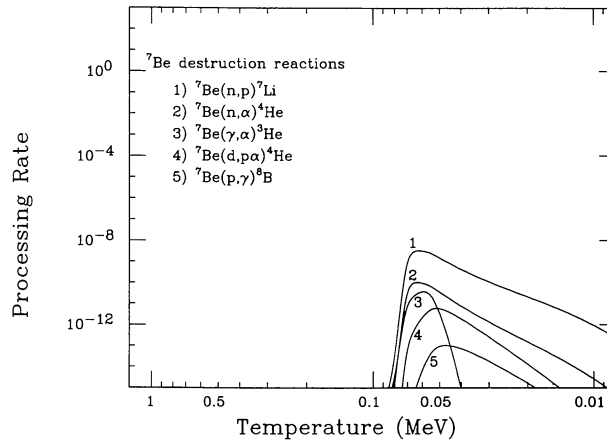


FIG. 9b

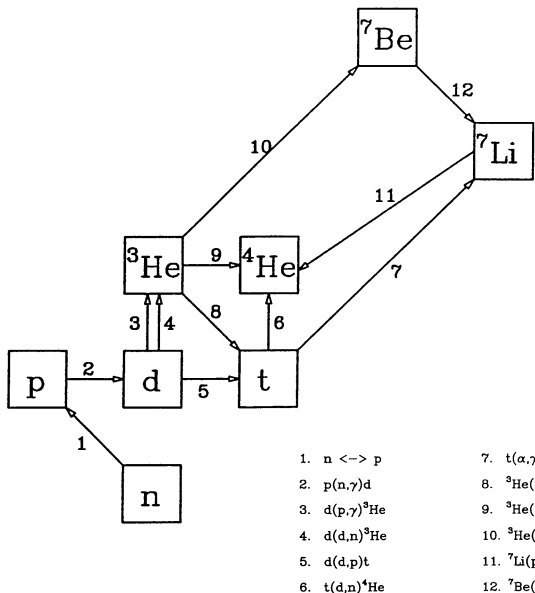


FIG. 10.—Network diagram of the 12 primary reactions in the processing of the light elements.

element abundances in the big bang occurs over the temperature range  $T \sim 0.01$  to  $0.1$  MeV, or  $T_9 \sim 0.1$  to  $1$ , where  $T_9$  is the temperature in  $10^9$  K ( $T = 1$  MeV corresponds to  $T_9 = 11.6$ ); see Figure 2. This is significantly higher than the temperature range for (nonexplosive) stellar nucleosynthetic processes of  $T_9 \sim 0.001$  to  $0.1$ .

The third purpose for undertaking our study is to determine the uncertainties of important SBBN reaction rates, which allow us to make robust light-element abundance predictions when incorporated into our Monte Carlo analysis. Rate uncertainties were first estimated for a number of reactions in 1967 in FCZI. These uncertainties ranged from 10% to a factor of 2 for temperatures up to  $T_9 = 10$ . The primordial nucleosynthesis studies of Yang et al. (1984) and Walker et al. (1991) used a recent unpublished estimate of reaction rate uncertainties by Fowler & Caughlan, while the studies of Beaudet & Reeves (1984), Delbourgo-Salvador et al. (1985), and Riley & Irvine (1991) relied primarily on the uncertainties of a few recent measurements of individual cross sections. Krauss & Romanelli (1990) made the first quantitative study of the uncertainties of reaction rates utilizing all available data. However, they discussed only those reactions which had been recently remeasured, and they did not determine the uncertainties of the important  $^3\text{He}(n, p)t$  and  $^3\text{He}(d, p)^4\text{He}$  reactions. This study will expand upon the work of Krauss and Romanelli to obtain appropriate reaction rates and uncertainties of the 12 reactions found in § 2 to be most important for the production of elements during primordial nucleosynthesis.

Finally, by making a comprehensive analysis of important SBBN reaction rates, we hope to indicate reactions which are ripe for further experimental and theoretical investigation.

### 3.2. Reaction Rate Formalism

We will begin by reviewing aspects of the conversion of laboratory cross section measurements to thermonuclear reaction

rates, emphasizing the differences in obtaining rates for primordial versus stellar nucleosynthesis studies. This conversion involves a thermal average of the product of the cross section  $\sigma(E)$  and relative velocity  $v$  over a Maxwell-Boltzmann velocity distribution, and can be written as

$$N_a \langle \sigma v \rangle \propto T^{-3/2} \int_0^{+\infty} \sigma(E) E \exp(-E/kT) dE, \quad (9)$$

where  $T$  is the temperature of the plasma,  $E$  is the energy (center of mass energies will be used unless otherwise noted),  $N_a$  is Avogadro's number, and  $N_a \langle \sigma v \rangle$  is the density-independent reaction rate. The derivation of this expression, complete with numerical constants, is given in FCZI. For charged-particle cross sections, which have an exponential energy dependence from the Coulomb barrier penetrability, the integrand in equation (9) is peaked at an effective energy  $E_o$  with a width  $\Delta E_o$ , where

$$E_o = 122A^{1/3}(Z_1 Z_2)^{2/3} T_9^{2/3} \text{ keV}, \quad (10)$$

$$\Delta E_o = 237A^{1/6}(Z_1 Z_2)^{1/3} T_9^{5/6} \text{ keV}, \quad (11)$$

and where  $A$  is the reduced mass and  $Z_i$  are the nuclear charges of the interacting species (Wagoner 1969); there is a corresponding effective energy range for neutron-induced reactions. It is crucially important to accurately know the cross section over the appropriate temperature-dependent energy range  $E_o \pm \Delta E_o$ , since this provides the dominant contribution to the thermal average in equation (9). From equations (10) and (11), it is clear that the important energy range for  $\sigma(E)$  is quite different for stellar and primordial nucleosynthesis. For example, the effective energy  $E_o$  and range  $E_o \pm \Delta E_o$  for the  $d(d, n)^3\text{He}$  reaction are 6 keV and 0.5–11 keV at  $T_9 = 0.01$ , 122 keV and 0–360 keV at  $T_9 = 1.0$ , and 360 keV and 0–1260 keV at  $T_9 = 5.0$ .

The exponential energy dependence of the Coulomb barrier penetrability makes charged-particle cross sections extremely small—and therefore difficult to measure—at energies below 100 keV. It is therefore necessary to extrapolate  $\sigma(E)$  to lower energies for use in equation (9). We can make this extrapolation more reliable by dividing out two known cross-section energy dependences, the  $s$ -wave ( $l=0$ ) Coulomb barrier penetrability and the geometric factor  $\pi \lambda^2 \propto E^{-1}$ , resulting in the factorization

$$\sigma(E) = \frac{S(E)}{E} \exp[-(E_g/E)^{1/2}], \quad (12)$$

where the constant  $E_g$  is the Gamow energy (see FCZI). The cross section factor, or astrophysical  $S$ -factor,  $S(E)$  defined in equation (12) has a slow energy variation which is more easily extrapolated to zero energy than is  $\sigma(E)$ . We can rewrite the reaction rate in equation (9) in terms of  $S(E)$  as

$$N_a \langle \sigma v \rangle \propto T^{-3/2} \int_0^{+\infty} S(E) \times \exp[-(E_g/E)^{1/2} - E/kT] dE. \quad (13)$$

We analyzed the nonresonant contributions to the reaction rates in this study by converting cross-section values to  $S$ -factor values via equation (12), fitting the  $S$ -factor as a smooth function of energy, and then analytically or numerically integrating equation (13) to get the rate as a function of temperature. It is important to use equations (10) and (11) in determining the energy range for the  $S$ -factor fit appropriate to primordial nucleosynthesis reaction rates. For example, a fit of the very low-energy  $d(d, n)^3\text{He}$   $S$ -factor (up to  $E = 160$  keV, Krauss et al. 1987) is suitable for the *stellar* reaction rate. However, *this fit is a factor of 2 (360) higher than the data at  $E = 360$  (1260) keV*, which is the top of the energy range  $E_o + \Delta E_o$  at  $T_9 = 1$  (5). The CF88 rate for this reaction, which is based on the low-energy fit, must therefore be modified for use in SBBN studies.

We will now examine the different expressions for  $S(E)$  used in equation (13) to determine the rates of the reactions important for SBBN.  $S(E)$  is often expanded in a Taylor series about zero energy because of its slow energy dependence, as

$$S(E) = S(0) \left[ 1 + \frac{S'(0)}{S(0)} E + \frac{1}{2} \frac{S''(0)}{S(0)} E^2 \right], \quad (14)$$

where  $S(0)$  is the value of  $S(E)$  at zero energy, and  $S'(0)$  and  $S''(0)$  are the first and second derivatives of  $S(E)$  with respect to energy evaluated at  $E = 0$ , respectively. When this polynomial  $S$ -factor expansion is inserted into equation (13), the thermal average can be done analytically, giving a reaction rate of the form

$$N_a \langle \sigma v \rangle \propto S(0) T^{-2/3} \exp(-aT^{-1/3}) \left( 1 + \sum_{n=1}^5 b_n T^{n/3} \right). \quad (15)$$

In this expression,  $a$  is a constant, and the relationship between the coefficients  $b_n$  and the derivatives  $S'(0)$  and  $S''(0)$  in equation (14) is given in FCZI. This polynomial parameterization of the  $S$ -factor, with coefficients determined by a least-squares fit to the data, is used to obtain the rates of the nonresonant charged-particle reactions  $d(p, \gamma)^3\text{He}$ ,  $d(d, n)^3\text{He}$ , and  $d(d, p)t$ , and for the nonresonant terms of the  $t(d, n)^4\text{He}$ ,  $^3\text{He}(d, p)^4\text{He}$ , and  $^7\text{Li}(p, \alpha)^4\text{He}$  reaction rates.

The nonresonant  $t(\alpha, \gamma)^7\text{Li}$  and  $^3\text{He}(\alpha, \gamma)^7\text{Be}$  reactions are predicted to have a combination of polynomial and decreasing exponential terms for  $S(E)$  through the results of the Resonating Group Method (RGM) calculations of Kajino, Toki, & Austin (1987). An exponentially decreasing  $S$ -factor of the form

$$S(E) = S(0) \exp(-aE), \quad (16)$$

for some constant  $a$ , corresponds to a reaction rate of the form

$$N_a \langle \sigma v \rangle \propto S(0) T^{-3/2} T_a^{5/6} \exp(-bT_a^{-1/3}), \quad (17)$$

where  $T_a = T/(1 + aT/c)$ , and  $b$  and  $c$  are constants.

The  $^3\text{He}(d, p)^4\text{He}$ ,  $t(d, n)^4\text{He}$ , and  $^7\text{Be}(n, p)^7\text{Li}$  reactions each have a broad cross section resonance at energies relevant to primordial nucleosynthesis, the contribution of which must be added to the nonresonant reaction rate. The thermal aver-

age of  $\sigma v$  over a *narrow* resonance (resonance width  $\ll$  energy spread of interacting particles  $\sim kT$ ) gives a reaction rate of the form

$$N_a \langle \sigma v \rangle \propto T^{-3/2} \omega \gamma \exp(-E_r/kT), \quad (18)$$

where  $\omega \gamma$  and  $E_r$  are the resonance strength and resonance energy, respectively. There is no equivalent simple expression for a broad resonance because of the significant energy variation of the entrance and exit channel widths. Broad resonances were treated in FCZII by first thermally averaging  $\sigma v$  numerically, and then fitting the resulting temperature-dependent function with an expression resembling the narrow resonance formula, where the resonance parameters in equation (18) are replaced by fit parameters. We used this approach with  $R$ -matrix fits of the resonant  $^3\text{He}(d, p)^4\text{He}$ ,  $t(d, n)^4\text{He}$ , and  $^7\text{Be}(n, p)^7\text{Li}$   $S$ -factors.

The nonresonant neutron-induced reactions  $p(n, \gamma)d$  and  $^3\text{He}(n, p)t$  must be treated separately from the charged-particle reactions because there is no Coulomb barrier penetrability term in their cross sections. In the simplest approximation for nonresonant reactions,  $\sigma \propto v^{-1}$ , so  $\sigma v$  is a constant. In general,  $R(E) = N_a \sigma v$  has a slow variation with energy, analogous to  $S(E)$  for charged-particle reactions. The slow energy variation allows us to use a polynomial expansion for  $R(E)$  in  $E^{1/2}$ :

$$R(E) = R(0) \left[ 1 + \sum_{n=1}^m \frac{1}{n!} \frac{R^{(n)}(0)}{R(0)} E^{n/2} \right], \quad (19)$$

where  $R^{(n)}(0)$  is the  $n^{\text{th}}$  derivative of  $R(E)$  with respect to energy evaluated at  $E = 0$ , and typically  $m \leq 5$ . The quantity  $R(0)$  is related to the thermal neutron capture cross section as described in FCZI. The thermal average of this expansion for  $R(E)$  over the Maxwell-Boltzmann velocity distribution is given by

$$N_a \langle \sigma v \rangle \propto R(0) \left( 1 + \sum_{n=1}^m C_n T^{n/2} \right). \quad (20)$$

The relationship of the coefficients  $C_n$  to the derivatives  $R^{(n)}(0)$  is given in FCZI for  $n = 1$  and 2; the general form is

$$C_n = \frac{R^{(n)}(0)}{R(0)} \frac{k^{n/2}}{n!} \frac{\Gamma[(n+3)/2]}{\Gamma(3/2)}, \quad (21)$$

where  $k$  is the Boltzmann constant and  $\Gamma(n)$  is the gamma function. This reaction rate form was used for the nonresonant  $p(n, \gamma)d$  and  $^3\text{He}(n, p)t$  reactions.

Finally, the nonresonant portion of the  $S$ -factor for the  $^7\text{Be}(n, p)^7\text{Li}$  reaction was fitted with a polynomial term (eq. [19]) plus a decreasing exponential,

$$R(E) = R(0) \exp(-aE), \quad (22)$$

where  $a$  is some constant. When thermally averaged, this exponential  $R(E)$  term gives a reaction rate of the form

$$N_a \langle \sigma v \rangle \propto R(0) T^{-3/2} T_a^{3/2}, \quad (23)$$

where  $T_a = T/(1 + aT/c)$ , and  $c$  is a constant.

The use of these equations in fitting the experimental data of each of the 12 individual reactions is discussed in detail in § 3.4, and the resulting reaction rates are listed in Table 1.

### 3.3. Reaction Rate Uncertainties

There are four contributions to the total reaction rate uncertainty: the statistical and systematic uncertainties of the laboratory cross section measurements, the uncertainty in the parameters of a smooth fit to the  $S$ -factor as a function of energy, and the uncertainty in an analytic approximation to the thermal average of  $\sigma v$ . Statistical uncertainties range from 2% to 20%, with more recent measurements giving (in general) greater precision; and fitting uncertainties are typically less than 5%. It is the systematic uncertainties, as evidenced by the scatter of the cross section values from different experiments, that typically provides the dominant contribution to the total uncertainty. For some reactions, different measurements barely overlap at the 2  $\sigma$  level; in these cases, a reasonable consideration of all of the data forces the total uncertainty to be significantly larger than that of the most precise measurement in the data set. In our efforts to eventually arrive at robust abundance

predictions, we have chosen conservative  $S$ -factor uncertainties such that most ( $\sim 95\%$ ) of the data are included at the 2  $\sigma$  level.

The  $S$ -factor uncertainty for a charged-particle reaction is often expressed as a fractional uncertainty in  $S(0)$  in equations (14) and (16); for a neutron-induced reaction, a fractional uncertainty in  $R(0)$  (eqs. [19] and [22]) is used. Since the reaction rate is proportional to  $S(0)$  [or  $R(0)$ ], an energy-independent fractional uncertainty in  $S(E)$  [or  $R(E)$ ] will result in the same temperature-independent fractional uncertainty in the reaction rate. Typically, the uncertainty in  $S(0)$  represents both the scatter of the data at laboratory energies as well as the difficulties in the extrapolation to zero energy; this is appropriate for  $E_o \sim 1-10$  keV, i.e., for stellar nucleosynthesis. For primordial nucleosynthesis, however,  $E_o \gtrsim 100$  keV, and it is therefore inappropriate to include the extrapolation uncertainty. With this in mind, we have assigned an energy-independent uncertainty characteristic of the  $S$ -factor uncertainty over  $E_o \pm \Delta E_o$  to all but two of the reactions under consideration. While we expressed this uncertainty as a fractional uncertainty in  $S(0)$ , it does not necessarily represent the actual uncertainty in  $S(E)$  at zero energy.

TABLE I  
NUCLEAR REACTION RATES<sup>a</sup>

Number	Reaction	Reference	Rate ( $\text{cm}^3 \text{s}^{-1} \text{mole}^{-1}$ )
1 .....	p(n, $\gamma$ )d	present	$4.742 \times 10^4 (1. - 0.850 T_9^{1/2} + 0.490 T_9 - 0.0962 T_9^{3/2} + 8.47 \times 10^{-3} T_9^2 - 2.80 \times 10^{-4} T_9^{5/2})$
2 .....	d(p, $\gamma$ ) <sup>3</sup> He	FCZII	$2.65 \times 10^3 T_9^{-2/3} \exp(-3.720/T_9^{1/3}) (1. + 0.112 T_9^{1/3} + 1.99 T_9^{2/3} + 1.56 T_9 + 0.162 T_9^{4/3} + 0.324 T_9^{5/3})$
3 .....	d(d, n) <sup>3</sup> He	present	$3.95 \times 10^8 T_9^{-2/3} \exp(-4.259/T_9^{1/3}) \times (1. + 0.098 T_9^{1/3} + 0.765 T_9^{2/3} + 0.525 T_9 + 9.61 \times 10^{-3} T_9^{4/3} + 0.0167 T_9^{5/3})$
4 .....	d(d, p)t	FCZII	$4.17 \times 10^8 T_9^{-2/3} \exp(-4.258/T_9^{1/3}) (1. + 0.098 T_9^{1/3} + 0.518 T_9^{2/3} + 0.355 T_9 - 0.010 T_9^{4/3} - 0.018 T_9^{5/3})$
5 .....	<sup>3</sup> He(n, p)t	present	$7.21 \times 10^8 (1. - 0.508 T_9^{1/2} + 0.228 T_9)$
6 .....	t(d, n) <sup>4</sup> He	present	$1.063 \times 10^{11} T_9^{-2/3} \exp[-4.559/T_9^{1/3} - (T_9/0.0754)^2] \times (1. + 0.092 T_9^{1/3} - 0.375 T_9^{2/3} - 0.242 T_9 + 33.82 T_9^{3/3} + 55.42 T_9^{5/3}) + 8.047 \times 10^8 T_9^{-2/3} \exp(-0.4857/T_9)$
7 .....	<sup>3</sup> He(d, p) <sup>4</sup> He	present	$5.021 \times 10^{10} T_9^{-2/3} \exp[-7.144/T_9^{1/3} - (T_9/0.270)^2] \times (1. + 0.058 T_9^{1/3} + 0.603 T_9^{2/3} + 0.245 T_9 + 6.97 T_9^{4/3} + 7.19 T_9^{5/3}) + 5.212 \times 10^8 / T_9^{1/2} \exp(-1.762/T_9)$
8 .....	<sup>3</sup> He( $\alpha$ , $\gamma$ ) <sup>7</sup> Be	present	$4.817 \times 10^6 T_9^{-2/3} \exp(-14.964/T_9^{1/3}) \times (1. + 0.0325 T_9^{1/3} - 1.04 \times 10^{-3} T_9^{2/3} - 2.37 \times 10^{-4} T_9 - 8.11 \times 10^{-5} T_9^{4/3} - 4.69 \times 10^{-5} T_9^{5/3}) + 5.938 \times 10^6 T_{9a}^{5/6} T_9^{-3/2} \exp(-12.859/T_9^{1/3})$ $T_{9a} = T_9/(1. + 0.1071 T_9)$
9 .....	t( $\alpha$ , $\gamma$ ) <sup>7</sup> Li	present	$3.032 \times 10^5 T_9^{-2/3} \exp(-8.090/T_9^{1/3}) \times (1. + 0.0516 T_9^{1/3} + 0.0229 T_9^{2/3} + 8.28 \times 10^{-3} T_9 - 3.28 \times 10^{-4} T_9^{4/3} - 3.01 \times 10^{-4} T_9^{5/3}) + 5.109 \times 10^5 T_{9a}^{5/6} T_9^{-3/2} \exp(-8.068/T_{9a}^{1/3})$ $T_{9a} = T_9/(1. + 0.1378 T_9)$
10 .....	<sup>7</sup> Be(n, p) <sup>7</sup> Li	present	$2.675 \times 10^9 (1. - 0.560 T_9^{1/2} + 0.170 T_9 - 0.0283 T_9^{3/2} + 2.21 \times 10^{-3} T_9^2 - 6.85 \times 10^{-5} T_9^{5/2}) + 9.391 \times 10^8 (T_{9a}/T_9)^{3/2} + 4.467 \times 10^7 T_9^{-3/2} \exp(-0.07486/T_9)$ $T_{9a} = T_9/(1. + 13.076 T_9)$
11 .....	<sup>7</sup> Li(p, $\alpha$ ) <sup>4</sup> He	present	$1.096 \times 10^9 T_9^{-2/3} \exp(-8.472/T_9^{1/3}) - 4.830 \times 10^8 T_{9a}^{5/6} T_9^{-3/2} \exp(-8.472/T_{9a}^{1/3}) + 1.06 \times 10^{10} T_9^{-3/2} \exp(-30.442/T_9) + 1.56 \times 10^5 T_9^{2/3} \exp[-8.472/T_9^{1/3} - (T_9/1.696)^2] \times (1. + 0.049 T_9^{1/3} - 2.498 T_9^{2/3} + 0.860 T_9 + 3.518 T_9^{4/3} + 3.08 T_9^{5/3}) + 1.55 \times 10^8 T_9^{-3/2} \exp(-4.478/T_9)$ $T_{9a} = T_9/(1. + 0.759 T_9)$
12 .....	Neutron decay	present	$\tau_n = 888.54 \text{ s}$

<sup>a</sup> Valid  $T_9$  range: 0.01–2 [Reactions 3, 4, 6, 7, 8, 9, 11]; 0.01–6 [Reactions 2, 5]; 0.01–20 [Reaction 10]; and 0.01–100 [Reaction 1].

The  $t(\alpha, \gamma)^7\text{Li}$  and  $^3\text{He}(\alpha, \gamma)^7\text{Be}$  reactions, however, require an energy-dependent uncertainty in  $S(E)$  because of large discrepancies in the low-energy behavior of  $S(E)$  from different experiments. These energy-dependent uncertainties in  $S(E)$  result in a temperature-dependent reaction rate uncertainty after thermal averaging. If a symmetric  $2\sigma$  uncertainty in  $S(E)$  is given by

$$S(E)_{\pm 2\sigma} = S(E)[1 \pm f(E)], \quad (24)$$

for some function  $f(E)$ , the corresponding thermally averaged reaction rates  $N_a \langle \sigma v \rangle_{\pm 2\sigma}$  are not symmetric about  $N_a \langle \sigma v \rangle$ . In order to ease the computational requirements in the Monte Carlo procedure described in § 4, the  $S$ -factor uncertainties were iteratively adjusted to produce the symmetric reaction rate uncertainty

$$N_a \langle \sigma v \rangle_{\pm 2\sigma} = N_a \langle \sigma v \rangle [1 \pm g(T)], \quad (25)$$

where the function  $g(T)$  is given as a polynomial expansion in  $T^{n/2}$ .

The uncertainty of each of the 12 important reactions is described in detail in the following sections, and a summary of the uncertainties is found in Table 2.

### 3.4. Individual Reaction Rates and Uncertainties

#### 3.4.1. The $p(n, \gamma)d$ Reaction

Essentially all deuterium is created by the  $p(n, \gamma)d$  reaction, as evident from Figure 4a. The analytic expression for this reaction rate has not changed since the FCZI compilation, which used theoretical calculations of deuteron photodissociation (Bethe & Morrison 1956, p. 75; Evans 1955) normalized to the thermal neutron capture cross section measurement of Hughes & Schwartz (1958) ( $\sigma_{th} = 0.332 \pm 0.002$  barn). The most recent  $p(n, \gamma)d$  evaluation is from Hale et al. (1991), who relied on the latest thermal neutron capture measurement of  $0.3326 \pm 0.006$  barn (Mughabghab et al. 1981), higher energy data (18–36 MeV) from Bosman et al. (1979), and deuteron photodissociation and neutron capture data from previous recent evaluations.

For energies  $E > 0.1$  MeV, there is a substantial discrepancy between the Hale et al. data evaluation and the FCZI expression for  $R(E) = N_a \sigma v$ , as evident from Figure 11. We have therefore made a new fit of  $R(E)$  to equation (19) with  $m = 5$  up to 25 MeV, to within 5% of Hale et al.;  $R(E)$  was taken as a constant for higher energies. This new fit is shown as the dashed line in Figure 11. The thermal average was found by numerical integration from 0.1 keV to 100 MeV at temperatures  $0.01 < T_9 < 100.0$  and was fit using equation (20) to within 2%. The final reaction rate is listed in Table 1. The uncertainty of the recommended cross section values, quoted from Hale et al., is 0.2%; previous compilations have higher uncertainties (Horsley 1966, 2%; Howerton 1959, 5%). We will assume a conservative 5% uncertainty in the evaluation, which, when combined in quadrature with the 5% fit of  $R(E)$  and the 2% fit of the numerical integration gives a total uncertainty of 7%.

#### 3.4.2. The $d(p, \gamma)^3\text{He}$ Reaction

The same analytic expression for the  $d(p, \gamma)^3\text{He}$  reaction rate is used in the FCZI, HFCZ, and CF88 tabulations, and is based on an  $S$ -factor fit to the very low energy (16–32 keV) data of Griffiths, Lal, & Scarfe (1963). Since this measurement used a thick heavy-ice target, the analysis required an assumed cross section energy dependence (approximated from a direct capture model) to extract the  $s$ -wave and  $p$ -wave cross sections from the measured thick-target yield. Two thin-target measurements, which require no assumed energy dependence, have been made at higher energies: Griffiths, Larson, & Robertson (1962) used thin ice and gas cell targets for  $180 < E < 1170$  keV; and Bailey et al. (1970) used thin deuterated-polyethylene and gas cell targets for  $35 < E < 740$  keV. These measurements, shown in Figure 12, are better represented by the polynomial  $S$ -factor (eq. [14]) used in FCZII (*solid curve*) than by the FCZI  $S$ -factor (*dotted curve*), so we chose to use the FCZII rate in our reaction network. For  $E > 350$  keV, a  $1\sigma$   $S$ -factor uncertainty of 5% is reasonable, but 10% is necessary at lower energies; this uncertainty is shown in Figure 12 by the dashed curves. Since the polynomial  $S$ -factor can be thermally aver-

TABLE 2  
NUCLEAR REACTION RATE UNCERTAINTIES

	Reaction	1 $\sigma$ Uncertainty (%)
1 .....	$p(n, \gamma)d$	7
2 .....	$d(p, \gamma)^3\text{He}$	10
3 .....	$d(d, n)^3\text{He}$	10
4 .....	$d(d, p)t$	10
5 .....	$^3\text{He}(n, p)t$	10
6 .....	$t(d, n)^4\text{He}$	8
7 .....	$^3\text{He}(d, p)^4\text{He}$	8
8 .....	$^3\text{He}(\alpha, \gamma)^7\text{Be}$	$T_9 \leq 10: (27. - 15.T_{9b}^{1/2} + 4.0T_{9b} - 0.25T_{9b}^{3/2} - 0.02T_{9b}^2),$ $(T_{9b} = T_9 + 0.783)$ $T_9 > 10: 9.7$
9 .....	$t(\alpha, \gamma)^7\text{Li}$	$T_9 \leq 10: (29. - 5.9T_{9b}^{1/2} - 7.2T_{9b} + 4.0T_{9b}^{3/2} - 0.56T_{9b}^2),$ $(T_{9b} = T_9 + 0.0419)$ $T_9 > 10: 8.1$
10 .....	$^7\text{Be}(n, p)^7\text{Li}$	9
11 .....	$^7\text{Li}(p, \alpha)^4\text{He}$	8
12 .....	Neutron decay	0.42

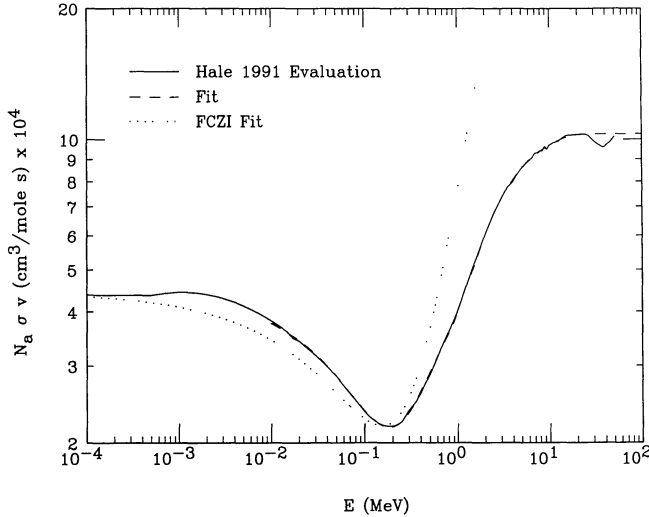


FIG. 11.— $p(n, \gamma)d$  data evaluation of Hale et al. (1991) and polynomial fits to  $R(E) = N_a \sigma v$  from the present work and from FCZI/CF88.

aged analytically (eq. [15]), the same conservative 10% uncertainty is appropriate for the reaction rate. A more precise measurement of this reaction would be very useful, since it is responsible for essentially all the  ${}^3\text{He}$  produced at high temperatures ( $T_9 > 3$ , Fig. 6a).

#### 3.4.3. The $d(d, n){}^3\text{He}$ Reaction

This reaction, the most important for  ${}^3\text{He}$  production at the peak nucleosynthesis temperature  $T_9 \approx 1$ , has been recently measured by Krauss et al. (1987) for  $E \leq 160$  keV and very precisely by Brown & Jarmie (1990) for  $E \leq 60$  keV. Previous measurements include Arnold et al. (1954) ( $E \leq 55$  keV) and Ganeev et al. (1957) ( $E \leq 1$  MeV). As stated in § 3.2, the polynomial S-factor fit (eq. [14]) of Krauss et al., used for the rate in the CF88 compilation, increases more rapidly with en-

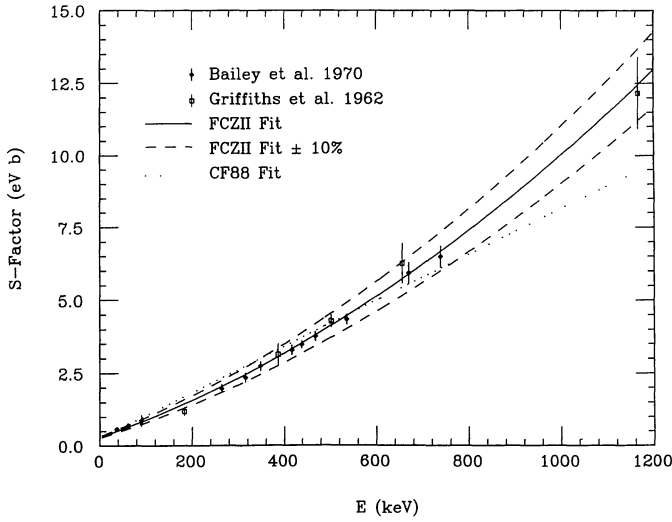


FIG. 12.— $d(p, \gamma){}^3\text{He}$  S-factor data and polynomial fits from FCZII and CF88. The dashed curves show the 1  $\sigma$  uncertainty of 10%.

ergy than the data for  $E > 150$  keV; the data and fit are shown in Figure 13. The polynomial S-factor fit used in FCZII is a good fit to the data for  $E < 300$  keV; however, their expression has  $S''(0) < 0$  in equation (14), leading to negative reaction rate values for  $T_9 > 20$  after  $S(E)$  is thermally averaged. Therefore, we have made a new polynomial S-factor fit with  $S''(0) > 0$  to the data from the four measurements listed above. This S-factor was thermally averaged analytically (eq. [15]) to get the  $d(d, n){}^3\text{He}$  reaction rate. Since the data of Brown & Jarmie, quoted to a precision of 1%–2%, differ by up to 10% from the measurements of Krauss et al. (with an uncertainty of 5%–8%), the total uncertainty must reflect the scatter of these two measurements. A conservative 1  $\sigma$  S-factor uncertainty of 10% includes all of the data up to 500 keV and is shown in Figure 13; this 10% uncertainty is appropriate for the  $d(d, n){}^3\text{He}$  reaction rate.

#### 3.4.4. The $d(d, p)t$ Reaction

This reaction, important for tritium production at  $T_9 \lesssim 1$ , was measured concurrently with the  $d(d, n){}^3\text{He}$  reaction in the studies of Brown & Jarmie (1990), Krauss et al. (1987), Ganeev et al. (1957), and Arnold et al. (1954); additional measurements have been made by Booth, Preston, & Shaw (1956), Preston, Shaw, & Young (1954), and McNeill & Keyser (1951). As with the  $d(d, n){}^3\text{He}$  reaction, the  $d(d, p)t$  S-factor fit used in CF88 (from Krauss et al.) increases more rapidly with energy than the data for  $E > 150$  keV, while the S-factor fit used by FCZII is a good fit to all of the data; the data and both fits are shown in Figure 14. Also similar to  $d(d, n)$ , the FCZII  $d(d, p)$  S-factor fit has  $S''(0) < 0$ . However, the  $d(d, p)$  reaction rate derived analytically from this S-factor is a good representation of the rate for all temperatures where tritium is produced via  $d(d, p)t$  ( $T_9 < 10$ ); therefore, this rate is used in our reaction network. A conservative 1  $\sigma$  uncertainty of 10% is necessary to include the scatter of all the S-factor data, as shown in Figure 14; this 10% uncertainty is also appropriate for the  $d(d, p)t$  reaction rate uncertainty.

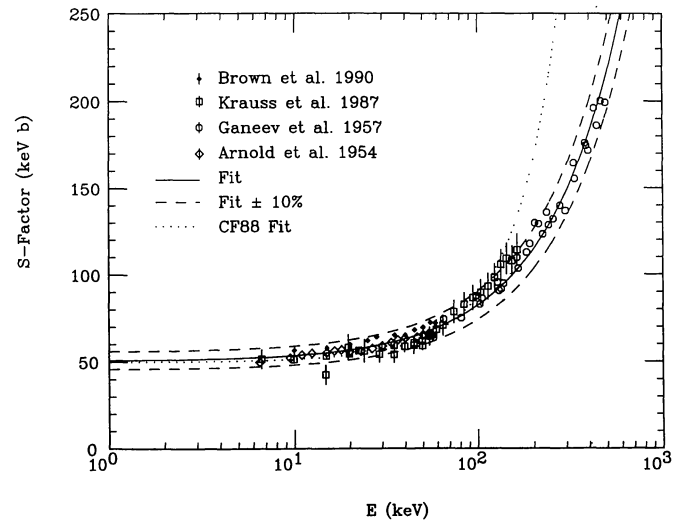


FIG. 13.— $d(d, n){}^3\text{He}$  S-factor data and polynomial fits from FCZII and CF88. The dashed curves show the 1  $\sigma$  uncertainty of 10%.

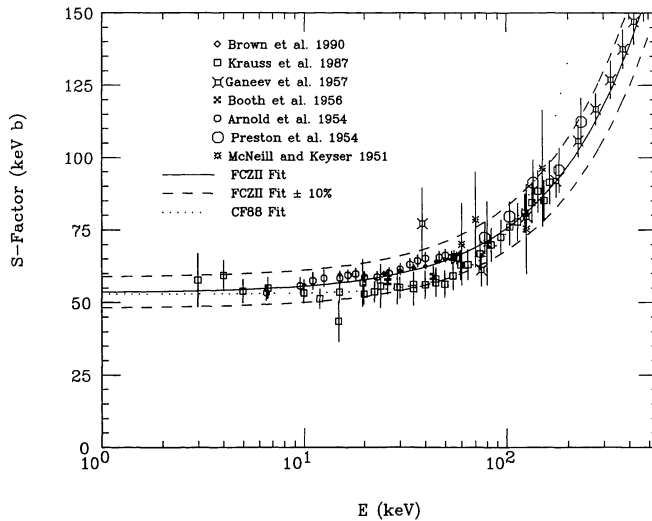


FIG. 14.— $d(d, p)t$  S-factor data and polynomial fits from FCZII and CF88. The dashed curves show the  $1\sigma$  uncertainty of 10%.

#### 3.4.5. The ${}^3He(n, p)t$ Reaction

This reaction, which maintains the  ${}^3He-t$  equilibrium at high temperatures, has been measured directly by Borzakov et al. (1982), Alfimenkov et al. (1980), Costello, Friesenhahn, & Lopez (1970), Batchelor, Aves, & Skyrme (1955), and Coon (1950); measurements of the inverse reaction  $t(p, n){}^3He$  have been made by Macklin & Gibbons (1965) and Gibbons & Macklin (1959). The thermal cross section has been precisely measured by Alfimenkov et al. to be  $5337 \pm 8$  barn. Figure 15 shows that the precise measurement of Borzakov et al. (2%–3%) lies below that of Alfimenkov et al. and Macklin and Gibbons for energies greater than 50 keV. The Borzakov et al. data also decrease more rapidly with energy than that from other measurements; however, this measurement does not extend past 100 keV, where other experiments indicate that  $R(E)$  begins to increase with energy.

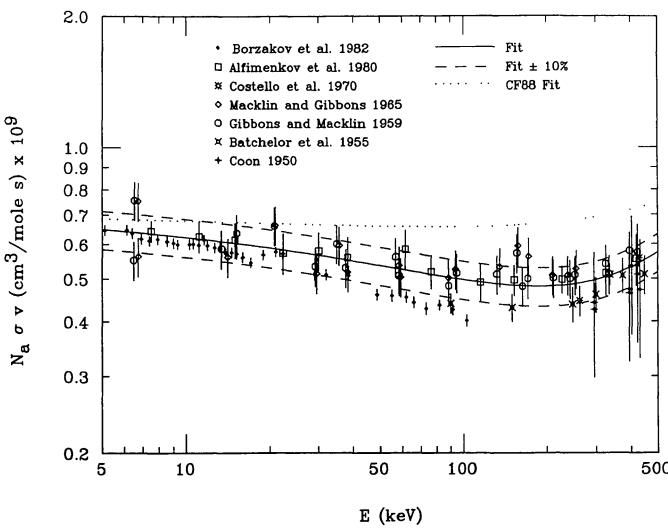


FIG. 15.—Data and polynomial fits to  $R(E) = N_a \sigma v$  from the present work and from CF88 for  ${}^3He(n, p)t$ . The dashed curves show the  $1\sigma$  uncertainty of 10%.

The FCZII (and CF88) reaction rate is based on a polynomial fit to  $R(E)$ , using equation (19) with  $m = 2$ . This fit, shown as the dotted curve in Figure 15, is higher than the data at energies greater than 40 keV and has a shallower minimum at 200 keV. Our new second-order polynomial fit to all the data up to 1 MeV, except those of Borzakov et al., is also shown in Figure 15. The Borzakov et al. data were excluded from the fit because their low uncertainty forces  $R(E)$  below the data at  $E > 100$  keV; however, the Borzakov et al. data are within 10% of this fit up to  $E = 50$  keV, and within 15% of the fit for  $E < 100$  keV. Since the data from all measurements lie within 20% of the fit, this was chosen as a conservative  $2\sigma$  uncertainty for  $R(E)$ . The polynomial form of  $R(E)$  was analytically integrated to get the reaction rate (listed in Table 1) with the form of equation (20); the 10%  $1\sigma$  uncertainty in  $R(E)$  is also appropriate for the reaction rate.

#### 3.4.6. The $t(d, n){}^4He$ Reaction

The  $t(d, n){}^4He$  reaction, which along with  ${}^3He(d, p){}^4He$  is responsible for the majority of  ${}^4He$  production (Fig. 7a), has been measured very precisely (to 2%) by Brown, Jarmie, & Hale (1987) and Jarmie, Brown, & Hardekopf (1984); previous measurements include Davidenko, Pogrebov, & Saukov (1957), Arnold et al. (1954), Argo et al. (1952), and Conner, Bonner, & Smith (1952). The evaluation of Liskien & Paulsen (1973) gives recommended cross section values and contains additional references. There is reasonably good agreement between measurements, as shown in Figure 16, with the exception of Bretscher & French (1949) and Jarvis & Roaf (1953), which are not plotted, and the low energy data of Davidenko et al.

As mentioned in § 3.2, the cross section for this reaction has a broad resonance, with a centroid at  $E = 64$  keV and a total width of  $76 \pm 12$  keV (Ajzenberg-Selove 1988). A number of  $S$ -factor fits have been made, including a single-level  $R$ -matrix fit by Jarmie et al., multilevel  $R$ -matrix and  $S$ -matrix fits by Brown et al., and single-level Breit-Wigner and  $R$ -matrix fits by Langanke & Rolfs (1989). We found that the single-level

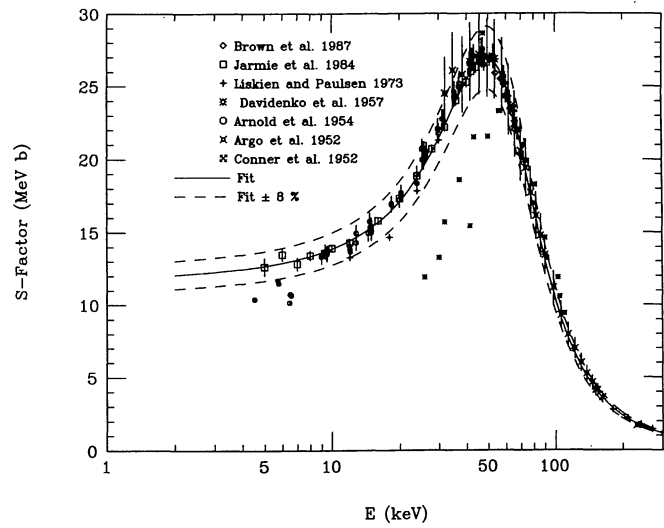


FIG. 16.— $t(d, n){}^4He$  S-factor data and  $R$ -matrix fit from the present work. The dashed curves show the  $1\sigma$  uncertainty of 8%.

*R*-matrix fit gives the best representation of the data up to 400 keV; the reduced width of the entrance channel was the only parameter changed from the fit of Jarmie et al. (to a value within their quoted uncertainty). We derived the thermal average of the *S*-factor by numerically integrating equation (13) from 1 keV to 1 MeV for temperatures  $0.01 < T_9 < 2$ . This was fit to within 2% of an analytic reaction rate consisting of a nonresonant term (eq. [15]) plus a resonant term (eq. [18]); the resulting rate is listed in Table 1. A  $1\sigma$  *S*-factor uncertainty of 5% is reasonable for  $E < 80$  keV, since the majority of the data are with 10% of the fit. For  $E > 80$  keV, there are no recent precise measurements, and an 8%  $1\sigma$  *S*-factor uncertainty is appropriate; we chose to use this more conservative value for the entire energy range. Combining the 8% *S*-factor uncertainty in quadrature with the 2% uncertainty of the fit to the integrated rate gives a total reaction rate uncertainty of  $\approx 8\%$ . A high-precision measurement of the  $t(d, n)^4\text{He}$  reaction at energies above the resonance could significantly decrease the overall *S*-factor uncertainty.

#### 3.4.7. The ${}^3\text{He}(d, p){}^4\text{He}$ Reaction

The  ${}^3\text{He}(d, p){}^4\text{He}$  reaction was treated in the same manner as its isobaric-analog reaction  $t(d, n){}^4\text{He}$ .  ${}^3\text{He}(d, p){}^4\text{He}$  has been measured by Krauss et al. (1987), Moller & Besenbacher (1980), Zhichang et al. (1977), and Arnold et al. (1954). The *S*-factor data are plotted in Figure 17; some scatter in the low-energy data is evident. The broad resonance in  ${}^3\text{He}(d, p){}^4\text{He}$  has a centroid at  $E = 258$  keV and a total width of  $200 \pm 60$  keV (Ajzenberg-Selove 1988). At energies below 40 keV, experiments have demonstrated that electron screening causes an increase in the *S*-factor with decreasing energy, of roughly 20% at 10 keV and up to 70% at 5 keV; details are given in Engstler et al. (1989), Schroder et al. (1989), Engstler et al. (1988), and Assenbaum, Langanke, & Rolfs (1987). Because the screening effect occurs only at very low energies, it has little influence on the reaction rate at primordial nucleosynthesis

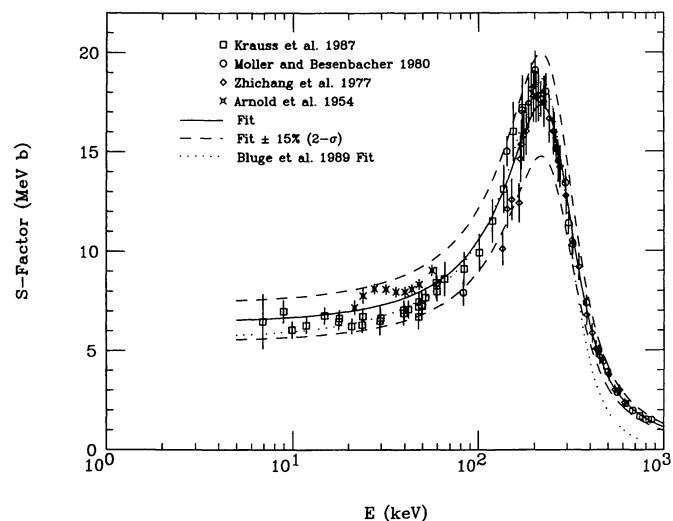


FIG. 17.— ${}^3\text{He}(d, p){}^4\text{He}$  *S*-factor data with *R*-matrix fit from the present work (solid curve) and Breit-Wigner fit from Bluge et al. (1989) (dotted curve). The dashed curves show the  $2\sigma$  uncertainty of 15%.

temperatures despite the substantial increases in  $S(E)$ —this effect will therefore not be included in the present analysis.

Bluge et al. (1989) made a single-level Breit-Wigner *S*-factor fit to the data based on RGM calculations of  ${}^3\text{He}(d, p){}^4\text{He}$ ; Bluge & Langanke (1990) made a similar fit based on a multi-channel RGM study of the levels of  ${}^5\text{Li}$ . However, as evident from the dotted curve in Figure 17, these fits do not well represent the data for energies  $E > 250$  keV. We fit the data up to 1 MeV with a resonant *S*-factor term similar to the *R*-matrix formulation used in Jarmie et al. (1984) for the  $t(d, n){}^4\text{He}$  reaction, added to a polynomial nonresonant *S*-factor term; the fit is shown by the solid curve in Figure 17. The thermal average of this *S*-factor was found by numerically integrating equation (13) from 1 keV to 1 MeV for temperature  $0.01 < T_9 < 2$ . This was fit to within 2% over this temperature range to an expression of the same form used for the  $t(d, n){}^4\text{He}$  reaction, resulting in the rate listed in Table 1. The *S*-factor fit includes all of the data within 15%, so a  $1\sigma$  uncertainty of 7.5% is reasonable. Adding in quadrature the 2% uncertainty in the fit of the rate expression gives a total  $1\sigma$  uncertainty of 8%.

#### 3.4.8. The ${}^3\text{He}(\alpha, \gamma){}^7\text{Be}$ Reaction

As evident from Figure 9a, the  ${}^3\text{He}(\alpha, \gamma){}^7\text{Be}$  reaction produces essentially all of the  ${}^7\text{Be}$  in the big bang; this decays (after the BBN epoch) to  ${}^7\text{Li}$ . The motivation for much of the experimental and extensive theoretical work on this reaction, however, has arisen from the strong dependence of the solar  ${}^8\text{B}$  neutrino flux on  $S(0)$  for this reaction. There have been six  ${}^3\text{He}(\alpha, \gamma){}^7\text{Be}$  capture  $\gamma$ -ray measurements, at energies ranging from 0.1 to 1.6 MeV, by Hilgemeier et al. (1988), Alexander et al. (1984), Krawinkel et al. (1982), Osborne et al. (1982), Nagatani, Dwarakanath, & Ashery (1969), and Parker & Kavanagh (1963). The rise of the  ${}^3\text{He}(\alpha, \gamma){}^7\text{Be}$  *S*-factor data with decreasing energy is shown in the plot of the capture  $\gamma$ -ray measurements in Figure 18. Hilgemeier et al. suggested multiplying the capture data of Krawinkel et al. by a factor of 1.4 to correct for the original density estimate of their gas jet target; this renormalization, used in the present analysis, brings the Krawinkel et al. data into agreement with the other capture measurements.

There have also been four “activation method” cross section measurements, detecting the delayed  ${}^7\text{Be}$  radioactivity in thick implantation targets, at energies ranging from 0.6 to 6.0 MeV: Robertson et al. (1983), Volk et al. (1983), Osborne et al. (1982), and Hilgemeier et al. These activation method experiments, which typically involve cross section measurements at only one or two energies, give consistently higher values of  $S(0)$  than the capture experiments, which usually involve a measurement of an excitation function. The weighted mean values of  $S(0)$  for the activation and the capture  $\gamma$ -ray experiments are given in Hilgemeier et al. as  $0.58 \pm 0.02$  and  $0.51 \pm 0.02$  keV barn, respectively. It is suggested by Hilgemeier et al. that the marginal  $2\sigma$  overlap of these two results may be due to the widely varying incident beam energies and implantation target types used for the activation studies. Until the discrepancy between the two techniques is experimentally resolved, we have followed the suggestion of Hilgemeier et al. and based our analysis on only the capture  $\gamma$ -ray measurements. Our resulting *S*-factor, however, is consistent with the low-energy activation method results at the  $2\sigma$  level.

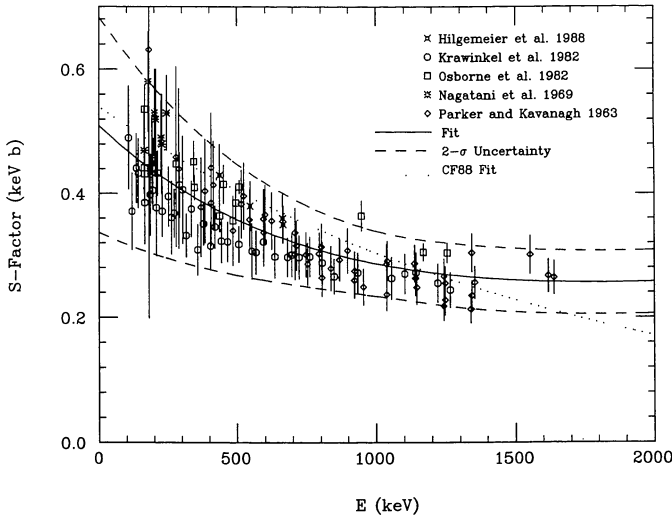


FIG. 18.— ${}^3\text{He}(\alpha, \gamma){}^7\text{Be}$  capture  $\gamma$ -ray  $S$ -factor data and fits from the present work and from CF88. The dashed curves show the energy-dependent  $2\sigma$   $S$ -factor uncertainty.

The analytic expressions for the  ${}^3\text{He}(\alpha, \gamma){}^7\text{Be}$  reaction rate in the FCZI and FCZII compilations are based on polynomial  $S$ -factor fits with  $S(0) = 0.47$  and  $0.61$  keV barn, respectively. Williams & Koonin (1981) used the direct-capture model of Christy & Duck (1961) to obtain an  $S$ -factor expression which decreases exponentially with energy (eq. [16]); this was subsequently used to obtain the reaction rates in HFCZ and CF88 with  $S(0) = 0.56$  and  $0.54$  keV barn, respectively. Kajino et al. (1987) made RGM calculations of both the  ${}^3\text{He}(\alpha, \gamma){}^7\text{Be}$  and  $t(\alpha, \gamma){}^7\text{Li}$  reactions, obtaining a polynomial times a decreasing exponential form for the  $S$ -factor. We fixed  $S(0) = 0.51$  keV barn, the weighted mean of the capture experiments, and made a new least-squares fit of the capture data up to  $E = 1.5$  MeV (including the renormalized data of Krawinkel et al.) to a polynomial plus a decreasing exponential, with the result

$$\begin{aligned} S(E) = & 0.51(1 + 1.071 \times 10^{-4}E) \\ & + 0.398[\exp(-1.198 \times 10^{-3}E) - 1] \text{ keV barn} \end{aligned} \quad (26)$$

for energies  $E$  in keV; above  $1.5$  MeV,  $S(E)$  was taken to be constant. This  $S$ -factor, written so that only the leading term contributes at  $E = 0$ , was thermally averaged by numerically integrating equation (13) from  $1$  keV to  $100$  MeV at temperatures  $0.01 < T_9 < 100.0$ . This was then fit to within  $4\%$  to equation (15) plus equation (17), giving the final reaction rate listed in Table 1. The uncertainty of this reaction rate for primordial nucleosynthesis studies could be reasonably characterized by a  $2\sigma$  fractional uncertainty in  $S(0)$  of approximately  $15\%$ . However, the uncertainty of the  $S$ -factor of the isobaric-analog reaction  $t(\alpha, \gamma){}^7\text{Li}$  requires an energy-dependent uncertainty due to discrepancies in the low-energy behavior of  $S(E)$ . We therefore chose to employ an energy-dependent  $S$ -factor uncertainty for both the  ${}^3\text{He}(\alpha, \gamma){}^7\text{Be}$  and  $t(\alpha, \gamma){}^7\text{Li}$  reactions. As mentioned in § 3.1, an iterative procedure, involving fitting  $\pm 2\sigma$   $S$ -factor curves followed by averaging and numerical integration followed by averaging, was employed to determine the symmetric reaction rate uncertainty

$N_a \langle \sigma v \rangle_{\pm 2\sigma}$  given in equation (25), where the function  $g(T)$  is

$$\begin{aligned} g(T) = & 0.541 - 0.301 T_{9b}^{1/2} + 0.0803 T_{9b} \\ & - 4.95 \times 10^{-3} T_{9b}^{3/2} - 3.97 \times 10^{-4} T_{9b}^2 \end{aligned} \quad (27)$$

for  $T_9 < 10$  ( $T_{9b} = T_9 + 0.783$ ), and  $g(T) = 0.195$  for  $T_9 > 10$ . This gives, for example,  $1\sigma$  reaction rate uncertainties of  $17\%$  at  $T_9 = 0.1$ ,  $14\%$  at  $T_9 = 1$ , and  $10\%$  for  $T_9 > 10$ .

### 3.4.9. The $t(\alpha, \gamma){}^7\text{Li}$ Reaction

This reaction, which produces  ${}^7\text{Li}$  directly during SBBN, was analyzed in the same manner as its isobaric-analog reaction,  ${}^3\text{He}(\alpha, \gamma){}^7\text{Be}$ . Because of the difficulty of fabricating tritium targets, there have been only three capture  $\gamma$ -ray measurements of  $t(\alpha, \gamma){}^7\text{Li}$  at energies ranging from  $0.08$  to  $1.8$  MeV: Schroder et al. (1987), Burzynski et al. (1987), and Griffiths et al. (1961). While the measurements of Griffiths et al. and Burzynski et al. are consistent with an energy-independent  $S$ -factor of  $0.064$  keV barn for  $E > 150$  keV, the measurement of Schroder et al. shows a substantial rise in  $S(E)$  with decreasing energy down to  $80$  keV: their extrapolation to zero energy yielded  $S(0) = 0.14 \pm 0.02$  keV barn, more than a factor of  $2$  larger than previous measurements. A preliminary result of a new capture  $\gamma$ -ray experiment by Brune, Kavanagh, & Rolfs (1992) confirms a rising  $S$ -factor with decreasing energy, although their  $S$ -factor rises less steeply than that of Schroder et al. Finally, a measurement has been made by Utsunomiya et al. (1990) employing the Coulomb breakup of  ${}^7\text{Li}$  via the  ${}^{208}\text{Pb}({}^7\text{Li}, \alpha t){}^{208}\text{Pb}$  reaction (and similar reactions with  ${}^{144}\text{Sm}$ ,  ${}^{120}\text{Sn}$ ,  ${}^{58}\text{Ni}$ , and  ${}^{27}\text{Al}$  targets) at  $6$  and  $9$  MeV  $\text{amu}^{-1}$ . Their data, normalized to Griffiths et al. at  $E = 500$  keV, exhibit the most rapid rise in  $S(E)$  with decreasing energy of all the experiments. The data from the four published experiments are plotted in Figure 19.

There are potential difficulties, however, with the interpretation of the results of Utsunomiya et al. First, there has been

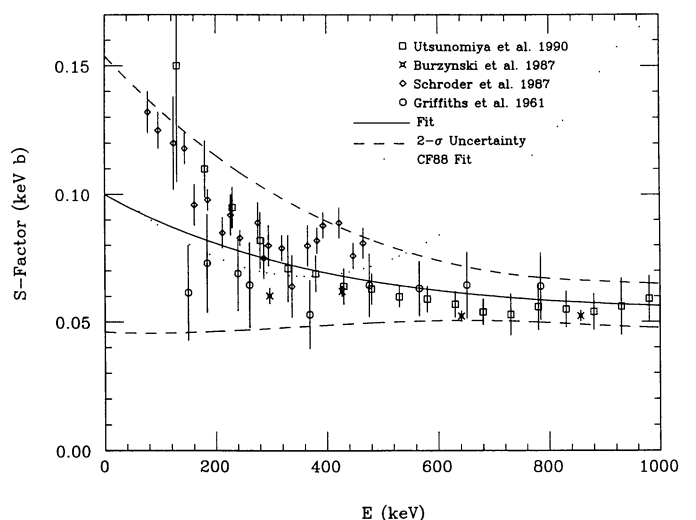


FIG. 19.— $t(\alpha, \gamma){}^7\text{Li}$   $S$ -factor data and fits from the present work and from CF88. The dashed curves show the energy-dependent  $2\sigma$   $S$ -factor uncertainty.

some question of the theory relating Coulomb-breakup data to radiative-capture rates as originally proposed by Baur, Bertulani, & Rebel (1986), especially the requirement that there be no interference between the Coulomb and nuclear contributions to the cross sections. This difficulty is much worse for nonresonant breakup reactions, such as  $t(\alpha, \gamma)^7\text{Li}$ , than for resonant breakup reactions. Measurements of Coulomb-breakup cross sections by Hill et al. (1991) indicate a smaller projectile-charge ( $Z$ ) dependence than predicted by calculation; the discrepancy increases with decreasing  $Z$ , with calculated cross sections a factor of 2 lower than measurements at  $Z = 6$  (the lowest  $Z$  studied). This suggests that artificially large capture cross sections may be predicted from the Coulomb-breakup technique. Measurements by Mason et al. (1992) of  $^{12}\text{C}$ ,  $^{197}\text{Au}(^7\text{Li}, \alpha t)$  at 8 MeV amu $^{-1}$  confirm that nuclear cross section effects are present, as well as target-proximity effects, in the breakup cross sections; see also Gazes et al. (1992).

There are also potential problems with the experiment of Schroder et al., but the extent of their influence on the  $S$ -factor energy dependence, of primary interest in this study, is uncertain. First, microscopic RGM calculations of the branching ratio of  $t + ^4\text{He}$  capture into the  ${}^7\text{Li}$  ground state ( $J^\pi = 3/2^-$ ) to  $t + ^4\text{He}$  capture into the  $E_x = 0.478$  MeV excited state ( $J^\pi = 1/2^-$ ) have been made by Altmeyer et al. (1988) and Kajino, Mathews, & Ikeda (1989). These calculations, which accurately predict the corresponding branching ratio in the analog  ${}^3\text{He}(\alpha, \gamma){}^7\text{Be}$  reaction, give  $t(\alpha, \gamma){}^7\text{Li}$  branching ratio values greater than 0.40 for a variety of nucleon-nucleon potentials ( $0.47 \pm 0.07$  from Kajino et al.). These estimates are consistent with the branching ratio values from Griffiths et al. ( $0.38 \pm 0.08$ ) and Burzynski et al. ( $0.50 \pm 0.04$ ), but are inconsistent with the  $0.32 \pm 0.01$  value from Schroder et al. Rolfs (1992) suggests that nonisotropic capture- $\gamma$ -ray angular distributions could lower this measured branching ratio: Schroder et al. assumed isotropy to 20% based on measurements at  $0^\circ$  and  $90^\circ$ , but the branching ratio could differ substantially if the two  ${}^7\text{Li}$  levels have different angular distributions. This would, however, have little effect on energy dependence of the total  $S$ -factor.

Finally, a recent measurement calls into question the tritium target thickness determined in the analysis of Schroder et al. and Griffiths et al. This has ramifications for the overall normalization of  $S(E)$  but not for the  $S$ -factor energy dependence. Schroder et al. calculated the target thickness by measuring yield from the  $t(p, \gamma){}^4\text{He}$  reaction at a proton energy  $E_p = 1$  MeV, assuming a cross section of  $30 \pm 2$   $\mu\text{barn}$  (Perry & Bame 1955); Griffiths et al. similarly employed the  $t(p, \gamma){}^4\text{He}$  yield at 800 keV. The target thicknesses found in this manner may have been underestimated, however, in view of a recent measurement of  $t(p, \gamma){}^4\text{He}$  for  $2 < E_p < 15$  MeV by Feldman et al. (1990), which gave a 35% lower result than previous studies. This implies that both Schroder et al. and Griffiths et al. may have overestimated their capture cross sections and  $S$ -factors. Since Burzynski et al. used the  $t(d, n){}^4\text{He}$  reaction to determine their tritium target thickness, their value is not influenced by the Feldman et al. result.

Until additional measurements of the  $S$ -factor energy dependence are made, the results of the Utsunomiya et al., Schroder et al., Burzynski et al., and Griffiths et al. will be used

to determine a new  $t(\alpha, \gamma){}^7\text{Li}$  reaction rate. The analytic expression for this rate in the FCZI and FCZII compilations was obtained from a constant  $S$ -factor equal to 0.064 keV barn from Griffiths et al. Langanke (1986) used a microscopic potential model for the  $S$ -factor which indicates a substantial rise in  $S(E)$  with decreasing energy, with an extrapolated value  $S(0) = 0.105$  keV barn. RGM calculations made by Kajino & Arima (1984), Mertelmeier & Hofmann (1986), Kajino (1986), and Kajino et al. (1987) also predict a rise in  $S(E)$  with decreasing energy. Kajino et al. derive a polynomial times a decreasing exponential form for the  $S$ -factor with an extrapolated value of  $S(0) = 0.100 \pm 0.025$  keV barn.

Langanke made a polynomial fit to his microscopic potential model  $S$ -factor at low energies to obtain the reaction rate used in CF88. As shown by the dotted curve in Figure 19, however, this polynomial fit is not appropriate for  $E \gtrsim 400$  keV. Since Figure 2 shows that processing of  ${}^7\text{Li}$  begins at temperatures of  $T \approx 0.1$  MeV ( $T_9 \approx 1$ ), where the effective energy range  $E_o \pm \Delta E_o$  is from 0 to 550 keV, the low-energy  $S$ -factor fit used for the CF88 rate should not be used for SBBN studies. We have therefore made a new least-squares fit of the  $S$ -factor data up to  $E = 2$  MeV, using a polynomial plus a decreasing exponential form and fixing the value of  $S(0)$  to be 0.100 keV barn; the result is

$$S(E) = 0.100(1 + 3.774 \times 10^{-5}E) + 0.0522[\exp(-2.411 \times 10^{-3}E) - 1] \text{ keV barn} \quad (28)$$

for energies  $E$  in keV. Above 2.0 MeV,  $S(E)$  is taken to be constant. This  $S$ -factor, shown as the solid curve in Figure 19, was thermally averaged by numerically integrating equation (13) from 1 keV to 100 MeV at temperatures  $0.01 < T_9 < 100.0$ , and was fit within 3% to equation (15) plus equation (17). The final reaction rate is given in Table 1, and is substantially smaller than the previous CF88 rate; the discrepancy is a factor of 2 at  $T_9 = 3$ . This indicates much less direct production of  ${}^7\text{Li}$  via  $t(\alpha, \gamma){}^7\text{Li}$  than previously estimated.

As discussed in § 3.4.8, this  $S$ -factor requires an energy-dependent uncertainty due to the large spread in values at low energies. The corresponding symmetric  $2\sigma$  reaction rate uncertainty (eq. [25]) was found in a fashion similar to that used for the  ${}^3\text{He}(\alpha, \gamma){}^7\text{Be}$  reaction. For  $t(\alpha, \gamma){}^7\text{Li}$ , the function  $g(T)$  in equation (25) was found to be

$$g(T) = 0.572 - 0.118T_{9b}^{1/2} - 0.145T_{9b} + 7.97 \times 10^{-2}T_{9b}^{3/2} - 1.11 \times 10^{-2}T_{9b}^2 \quad (29)$$

for  $T_9 < 10$ , where  $T_{9b} = T_9 + 0.0419$ , and  $g(T) = 0.161$  for  $T_9 > 10$ . This is plotted in Figure 19 as the dashed curve. This gives, for example,  $1\sigma$  reaction rate uncertainties of 26% at  $T_9 = 0.01$ , 19% at  $T_9 = 1$ , and 8% at  $T_9 > 10$ .

#### 3.4.10. The ${}^7\text{Be}(n, p){}^7\text{Li}$ Reaction

The conversion of  ${}^7\text{Be}$  to  ${}^7\text{Li}$  occurs both during nucleosynthesis, via the  ${}^7\text{Be}(n, p){}^7\text{Li}$  reaction, and after nucleosynthesis ends, via the 53 day half-life  ${}^7\text{Be}(e^+ \nu_e){}^7\text{Li}$  decay.  ${}^7\text{Be}(n, p){}^7\text{Li}$  has recently been directly measured by Koehler et al. (1988) from thermal neutron energies (25 meV) up to  $E_n =$

13.5 keV and by Andrzejewski et al. (1991) at  $E_n = 24.5$  keV. For energies from 10 keV to 3 MeV, it is necessary to use data from inverse  $^7\text{Li}(\text{p}, \text{n})^7\text{Be}$  measurements by Macklin & Gibbons (1958) and Gibbons & Macklin (1959), as tabulated in Kim et al. (1966). The data, shown in Figure 20, are in good agreement except for the lowest energy data points of Macklin and Gibbons which were measured very near the threshold of the inverse reaction. The high-precision thermal cross section value of Koehler et al.,  $\sigma_{th} = (3.882 \pm 0.0809) \times 10^4$  barn, dominates the weighted mean of all thermal measurements and agrees with one previous result (Brugger 1957) while being roughly 25% lower than some previous values (Cervena et al. 1989; Gledenov et al. 1986; Hanna 1955). This new  $\sigma_{th}$ -value significantly decreases  $R(E) = N_a \sigma v$  for  $E \lesssim 100$  keV (up to 25%) from the  $S$ -factor calculation of Bahcall & Fowler (1969) used for the FCZII rate.

The inverse measurements indicate a broad resonance with total width of 220 keV at  $E = 323$  keV (a laboratory proton energy of  $E_p = 2.25$  MeV) which affects the reaction rate at primordial nucleosynthesis temperatures. For energies  $E \leq 1$  MeV,  $R(E)$  was fit with a resonant  $R$ -matrix term plus a nonresonant third-order polynomial term (eq. [19]) and a nonresonant decaying exponential term (eq. [22]). For  $1.0 < E < 3.0$  MeV, the low-energy tail of a second  $^7\text{Li}(\text{p}, \text{n})^7\text{Be}$  resonance, at  $E_p = 4.975$  MeV, was fitted with a polynomial;  $R(E)$  was approximated by a constant for  $E > 3.0$  MeV. The fit is shown in Figure 20; a 1  $\sigma$  uncertainty of 6% is appropriate for data up to 3 MeV.  $R(E)$  was thermally averaged numerically from 1 keV to 100 MeV at temperatures  $0.01 < T_9 < 100.0$  and was fit with two nonresonant terms, equations (20) and (23), plus one resonant term, equation (18). The resulting analytic expression, listed in Table 1, agrees to within 6% of the numerical integration. The resonant term significantly affects the reaction rate for temperatures  $0.01 < T_9 < 1.0$ . The uncertainty of 6% from the fit of  $R(E)$  added in quadrature to 6% from the reaction rate fit gives a total reaction rate uncertainty of 9%.

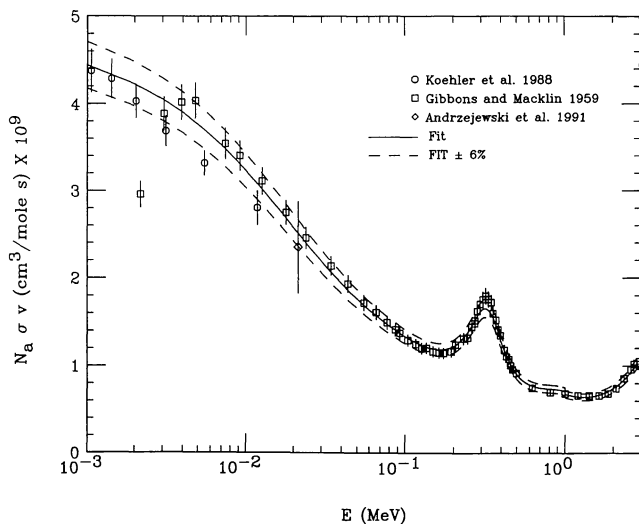


FIG. 20.—Data and polynomial fits to  $R(E) = N_a \sigma v$  from the present work for  $^7\text{Be}(\text{n}, \text{p})^7\text{Li}$ . The dashed curves show the 1  $\sigma$  uncertainty of 6%.

### 3.4.11. The $^7\text{Li}(\text{p}, \alpha)^4\text{He}$ Reaction

This reaction is the primary destruction mechanism for  $^7\text{Li}$  (Fig. 8b). It has been measured by Rolfs & Kavanagh (1986) for  $E = 25$ –875 keV, by Spinka, Tombrello, & Winkler (1971) for  $E = 115$ –490 keV, and by Harmon (1989) for  $E = 15$ –220 keV. As shown in Figure 21, the data from these three measurements are in good agreement, except for the 60–100 keV data of Harmon. Figure 21 also shows the CF88 fit to the data of Rolfs and Kavanagh,

$$S(E) = 52.0$$

$$+ 41.0[1 - \exp(-8.804 \times 10^{-3}E)] \text{ keV barn , } \quad (30)$$

where the energy  $E$  is in keV. Equation (30) is a good fit to the data, and this  $S$ -factor contributes terms of the form of equations (15) and (17) to the  $^7\text{Li}(\text{p}, \alpha)^4\text{He}$  reaction rate. There is an additional resonant reaction rate term, equation (18), for captures proceeding through the 2.623 MeV  $^8\text{Be}$  resonance ( $E_x = 19.86$  MeV, Ajzenberg-Selove 1988). The plot of the reaction rate, Figure 22, shows that the resonant  $^7\text{Li}(\text{p}, \alpha)^4\text{He}$  term contributes significantly to the total reaction rate only for  $T_9 > 4$ , temperatures where  $^7\text{Li}$  has not yet been formed (Fig. 2); the two nonresonant terms dominate the reaction rate for  $T_9 < 1$ . CF88 treats the  $^7\text{Li}(\text{p}, \gamma)^8\text{Be}$  reaction, where  $^8\text{Be}$  excited states undergo  $\gamma$ -decay before breaking up into two  $\alpha$ -particles, separately from the  $^7\text{Li}(\text{p}, \alpha)^4\text{He}$  reaction rate. Since both processes contribute to the rate of  $^7\text{Li}$  plus a proton forming two  $\alpha$ -particles ( $^7\text{Li} + \text{p} \rightarrow \alpha + \alpha$ ), the  $^7\text{Li}(\text{p}, \gamma)^8\text{Be}$  reaction rate must be added to the above  $^7\text{Li}(\text{p}, \alpha)^4\text{He}$  reaction rate to obtain the total reaction rate. The  $^7\text{Li}(\text{p}, \gamma)^8\text{Be}$  rate has a resonant contribution, from the 0.386 MeV  $^8\text{Be}$  state ( $E_x = 17.640$  MeV), and a nonresonant contribution, equation (15), from the low-energy tail of this same resonance. These  $^7\text{Li}(\text{p}, \gamma)^8\text{Be}$  terms were not included in the total  $^7\text{Li} + \text{p} \rightarrow \alpha + \alpha$  rate used in the previous version of the primordial nucleosynthesis program; their inclusion causes (at most) an 8% increase (at  $T_9 = 1$ ) from the previous  $^7\text{Li} + \text{p}$  burning rate. A 1  $\sigma$  uncertainty of 8% for  $S(E)$ , as measured by Rolfs and Kavanagh, is shown in Figure 21 and is a good estimate of the uncertainty of the total reaction rate.

### 3.4.12. Neutron Decay

The lifetime  $\tau_n$  of the free neutron decay  $\text{n} \rightarrow \text{p} + \text{e}^- + \bar{\nu}_e$  characterizes the strength of the neutron-proton weak interaction; the competition of this weak interaction rate with the expansion rate of the universe determines the amount of  $^4\text{He}$  produced during primordial nucleosynthesis (as described in § 2.1). A detailed discussion of the cosmological implications of the neutron lifetime can be found in Olive et al. (1981) and Schramm & Kawano (1989). Recent lifetime measurements have produced lower values of the neutron lifetime, implying less primordial  $^4\text{He}$  production. Lifetime experiments have traditionally utilized an in-beam method, where decay products (electrons or protons) are counted near a slow neutron beam (see the reviews of Dubbers 1991, Freedman 1990, and Byrne 1982); a newer set of experiments have utilized neutron storage devices (traps), in which the number of neutrons surviving in a trap are counted as a function of time. Storage

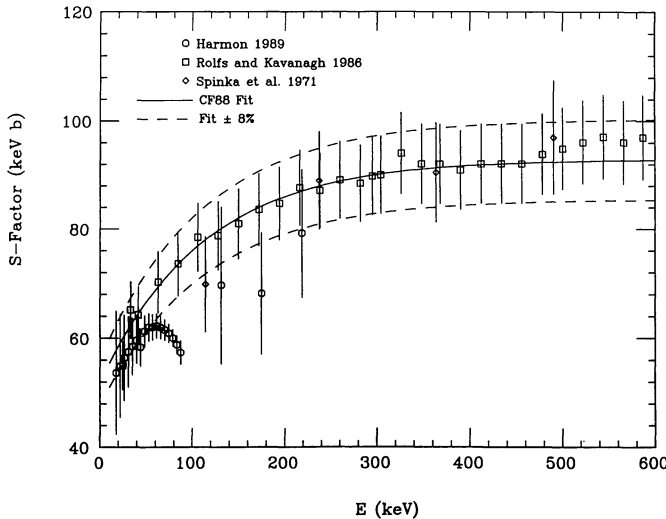


FIG. 21.— ${}^7\text{Li}(\text{p}, \alpha){}^4\text{He}$  S-factor data and fit from CF88. The dashed curves show the  $1\sigma$  uncertainty of 8%.

methods have exploited, for example, the neutron magnetic moment and the reflection properties of ultracold walls. Significant reductions in systematic uncertainties of trap methods have yielded the most precise lifetime measurements to date. A list of the measurements is given in Table 3; a list of very early and preliminary measurements is provided for completeness. An ideogram of the measurements, similar to that given in Freedman, is shown in Figure 23. In light of the recent use of a pulsed neutron beam (Last et al. 1988) and the significant experimental advances in trap techniques since 1986, we have followed Freedman and used a weighted mean of all lifetime measurements since 1986 ( $888.5 \pm 3.8$  s,  $2\sigma$ ). To account for systematic uncertainties in the measurements, we have doubled this purely statistical uncertainty in our Monte Carlo analysis (see § 4). The Spivak (1988) reanalysis of the Bondarenko et al. (1978) measurement was omitted from the mean of the recent measurements. The average of all measurements is  $889.8 \pm 3.6$  s, agreeing within errors with the mean of the recent measurements. We note that the Particle Data Group has recommended a value of  $889.1 \pm 2.1$  s (Hikasa et al. 1992), based on seven recent measurements and the values from Spivak (1988) and Christensen et al. (1972).

It should be noted that we have not included an estimate of  $\tau_n$  based on angular correlation measurements and weak coupling constant values, as done in Krauss & Romanelli (1990). Before the recent experimental advances in direct lifetime measurements, the most precise value for  $\tau_n$  was obtained from the vector and axial vector coupling constants  $G_V$  and  $G_A$ , or equivalently from  $G_V$  and  $\lambda = G_A/G_V$  (Dubbers 1991). Measurements of the electron-neutrino asymmetry  $a$ , beta asymmetry  $A$ , or neutrino asymmetry  $B$  are used to determine  $\lambda$ , while  $G_V$  can be determined from measurements of superallowed  $0^+ \rightarrow 0^+$  Fermi  $\beta$ -decay. Such estimates of  $\tau_n$ , however, assume a pure  $V - A$  theory to relate the asymmetry parameters  $a$ ,  $A$ , and  $B$  to  $\lambda$ , and also assume the validity of the conserved weak vector current (CVC) hypothesis to relate  $G_V$  for Fermi decays to  $G_V$  for neutron decay. Because of the recent precise direct measurements of  $\tau_n$ , and because the theoretical issues are still

being tested experimentally, we have chosen to utilize only direct measurements to obtain our weighted mean value of  $\tau_n$ .

### 3.5. Comparison of New and Previous Rates

In order to compare the rates used in our reaction network and Monte Carlo analysis with the CF88 rates, we have plotted the fractional rate difference (CF88 rate – present rate/present rate) as a function of temperature in Figures 24, 25, and 26. Over the important temperature range  $T_9 = 0.1$  to 10, the  $d(\text{p}, \gamma){}^3\text{He}$ ,  $t(\text{d}, n){}^4\text{He}$ ,  ${}^3\text{He}(\text{d}, p){}^4\text{He}$ ,  ${}^3\text{He}(\alpha, \gamma){}^7\text{Be}$ ,  ${}^7\text{Li}(\text{p}, \alpha){}^4\text{He}$ , and  ${}^7\text{Be}(\text{n}, \text{p}){}^7\text{Li}$  reactions differ by less than 20% from the corresponding CF88 rate. However, we find significantly lower rates for the  $\text{p}(\text{n}, \gamma)\text{d}$ ,  $d(\text{d}, n){}^3\text{He}$ ,  $d(\text{d}, p)t$ , and  $t(\alpha, \gamma){}^7\text{Li}$  reactions: the new rates are more than a factor of 2 lower than the CF88 rates for temperatures  $T_9 \gtrsim 7, 2, 2$ , and 3, respectively. The effect that these new rates have on the predicted abundances will be discussed at the end of § 4.

## 4. NUMERICAL ANALYSIS AND RESULTS

The overall effect of the reaction uncertainties listed in Table 2 on light-element abundances was determined by a Monte Carlo analysis similar to that of Krauss & Romanelli (1990). We represented each of the 12 major reaction rates by a Gaussian distribution centered on a mean rate value, listed in Table 1, with a width given by the rate uncertainty, listed in Table 2. In contrast with Krauss and Romanelli, we incorporated temperature-dependent reaction rate uncertainties where necessary. For a particular computer run, we employed a random number generator to select a number for each of the 12 reactions. This random number was used to determine a reaction rate whose distribution over many runs would give a Gaussian around the mean rate with a width equal to the  $1\sigma$  rate uncertainty found in § 3. The random number generated a displacement from the mean reaction rate via tabulated values of the distribution function; we ensured the positive-definiteness of the reaction rate by not generating uncertainties larger than 2.6

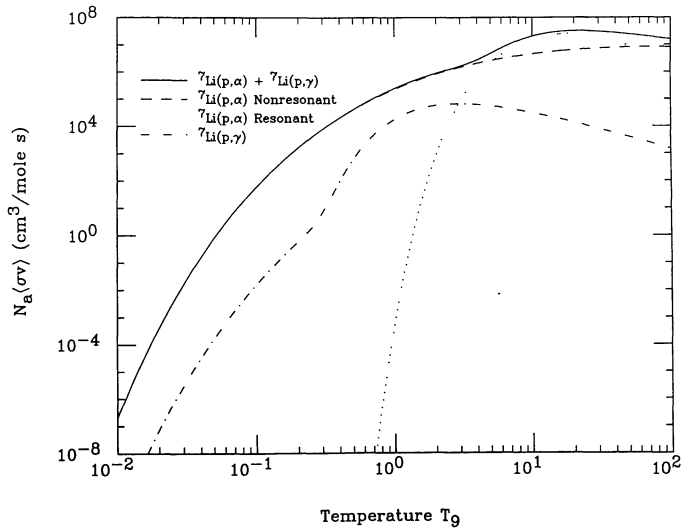


FIG. 22.—Total  ${}^7\text{Li} + \text{p} \rightarrow \alpha + \alpha$  reaction rate as a function of temperature, with contributions from both  ${}^7\text{Li}(\text{p}, \alpha){}^4\text{He}$  and  ${}^7\text{Li}(\text{p}, \gamma){}^8\text{Be}$ .

TABLE 3  
NEUTRON LIFETIME MEASUREMENTS

Reference	Lifetime (s)	Comment
Robson 1951 .....	1108±216	proton-electron coincidences
Spivak et al. 1956 .....	1039±130	early in-beam experiment
D'Angelo 1959 .....	1099±164	cloud chamber
Sosnovski et al. 1959 .....	1013±26	in-beam
Christensen et al. 1972 .....	918±14	in-beam
Paul & Trinks 1978 .....	909±69	early magnetic n-trap
Kosvintsev et al. 1980 .....	875±95	early material bottle n-trap
Kosvintsev et al. 1986 .....	903±13	n-trap; ultracold Al-walled cylinder
Kosvintsev et al. 1987 .....	893±20	n-trap; ultracold ice-walled cylinder
Last et al. 1988, Dohner et al. 1989 .....	876±21	pulsed n-beam; solenoid $e^-$ spectrometer
Spivak 1988 .....	891±9	in-beam; proton detection; reanalysis of Bondarenko et al. 1978
Anton et al. 1989, Paul et al. 1989 .....	877±10	n-trap; magnetic sextupole
Schreckenbach et al. 1989, Kossakowski et al. 1989 .....	878±30	in-beam; $e^-$ detection with TPC
Mampe et al. 1989 .....	887.6±3.0	n-trap; fluid-walled bottle
Byrne et al. 1990 .....	893.6±5.3	in-beam; Penning trap for protons
Alfimenkov et al. 1990 .....	888.4±2.9	n-trap; gravitational
Weighted mean, all .....	889.8±3.6	2 $\sigma$ uncertainty
Weighted mean, 1986–present .....	888.5±3.8	2 $\sigma$ uncertainty; without Spivak 1988
Preliminary Measurements		
Snell & Miller 1948 .....	>900	
Snell et al. 1950 .....	600–1800	
Robson 1950a .....	540–1080	superceded by Robson 1951
Robson 1950b .....	540–1500	superceded by Robson 1951
Christensen et al. 1967 .....	933±7	superceded by Christensen et al. 1972
Kugler et al. 1978 .....	918±138	superceded by Paul & Trinks 1978
Bondarenko et al. 1978 .....	877±8	reanalyzed in Spivak 1988
Byrne et al. 1980 .....	937±18	superceded by Byrne et al. 1990
Bondarenko 1982 .....	881±8	reanalyzed in Spivak 1988
Ageron et al. 1986 .....	850±60	superceded by Mampe et al. 1989
Kharitonov et al. 1989 .....	870±8	superceded by Alfimenkov et al. 1990

$\sigma$ . We incorporated these features into the latest adaptation of Wagoner's code (Kawano 1992), along with the 12 reaction rates discussed in § 3 and the (other unchanged) rates from CF88. We then computed the light-element abundances, compensating for computational errors associated with the linearizations in the Runge-Kutta method and in the abundance-changing differential equation; these corrections are discussed in Kawano (1992), and can be as great as 6%. We also corrected the  $^4\text{He}$  mass fraction by subtracting 0.0025 to account for an analytic approximation to the  $\text{p} \leftrightarrow \text{n}$  rates (Dicus et al. 1982).

For each value of the baryon-to-photon ratio  $\eta$ , the free parameter in SBBN, we did 1000 runs of the computer program and represented the results by a mean value and a 2  $\sigma$  standard deviation of the abundances of D,  $^3\text{He}$ ,  $^4\text{He}$ , and  $^7\text{Li}$ . We covered the range in  $\eta_{10}$  from 1 to 10 with 15 values, using a higher density of points around the  $^7\text{Li}$  “dip” near  $\eta_{10} = 3$ . In light of the recent analysis of  $Z_0$  width at CERN giving three neutrino species (summarized in Krauss 1991), we have confined our computations to the (standard model) case of three relativistic neutrino families.

We then plotted this information in a form that could be readily compared with observational data. Figure 27a shows the computed abundance for  $^4\text{He}$  (mass fraction  $Y_p$ ) plotted

against the baryon-to-photon ratio  $\eta$ , Figure 27b shows both  $(\text{D} + ^3\text{He})/\text{H}$  and  $\text{D}/\text{H}$ , and Figure 27c gives  $^7\text{Li}/\text{H}$  plotted against  $\eta$ . The continuous curves give the mean computed values for the elemental abundances, and the dashed lines give the 2  $\sigma$  abundance curves. In Figure 27b, the upper curve is for  $(\text{D} + ^3\text{He})/\text{H}$ , the lower for  $\text{D}/\text{H}$ , and the dotted lines give the 2  $\sigma$  curves for  $\text{D}/\text{H}$ . The boxes and other lines show the abundance constraints from observations listed in Table 5, discussed in § 5.

Before discussing these constraints, we can examine the effect of the new reaction rates. Table 4 lists the percent difference in the predicted abundances of D,  $^3\text{He}$ ,  $^4\text{He}$ , and  $^7\text{Li}$  as each of the reaction rates (excluding neutron decay) are individually changed from the CF88 rate to the new rate and as all rates are changed simultaneously. This is done for low (1.0), intermediate (3.0), and high (6.0) values of  $\eta_{10}$ . We see that, when the new reaction rates are used, the predicted abundances of D,  $^3\text{He}$ , and  $^7\text{Li}$  are changed by up to 20%. *Most importantly, the abundance of  $^7\text{Li}$  at high  $\eta$  values is predicted to be approximately 20% lower with the new rates;* as we will see in § 6, this will substantially affect the  $^7\text{Li}$  constraint on  $\eta$ . From Table 4, it is clear that this change is not due to any one particular reaction, but rather to the cumulative effect of changes in all 12 reactions.

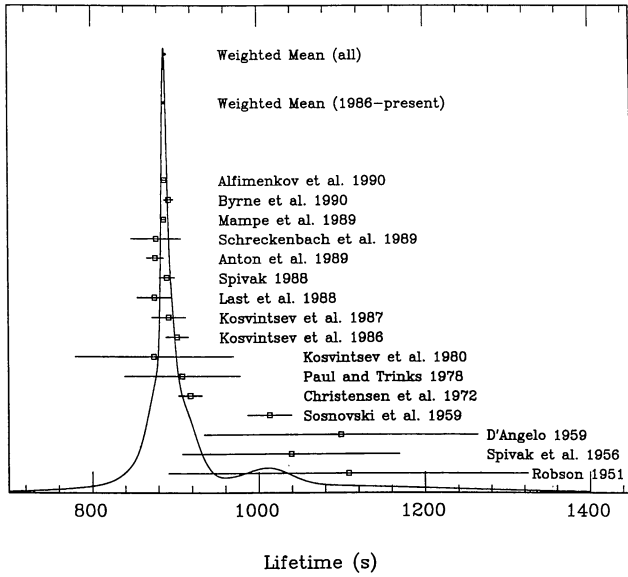


FIG. 23.—Ideogram of the neutron lifetime experimental data as in Freedman (1990). The curve is a sum of 16 equal-area Gaussians, one centered on each lifetime value with a width equal to that value's uncertainty. The weighted mean of all measurements and that of the recent measurements (1986–present) are also shown.

In our conservative approach, we have doubled the statistical uncertainty in  $\tau_n$  (Table 3) in our Monte Carlo analysis to account for systematic uncertainties in the measurements. If the purely statistical uncertainty ( $1\sigma$  of 1.9 s) is used instead, the resulting  $\pm 2\sigma$  abundance curves in Figure 27a are each shifted towards the mean abundance curve by  $Y_p \approx 0.0007$  for  $\eta_{10} \approx 4$ . This has a very small effect on the  $\eta$  upper bound obtained from the  $^4\text{He}$  abundance (see § 6), decreasing it by less than 6%, and an equally small effect on the  $\Omega_b$  upper bound. We have therefore used the larger uncertainty in keeping with our use of conservative rate uncertainties and abundance limits.

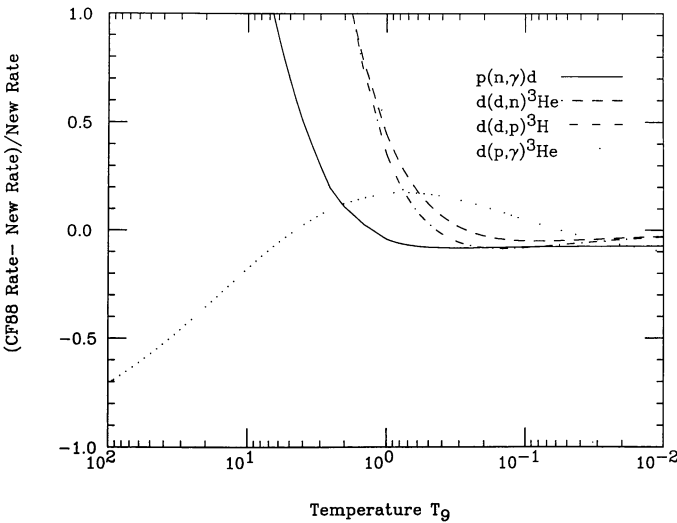


FIG. 24.—Fractional reaction rate difference (CF88 rate – present rate/present rate) as a function of temperature for the  $p(n, \gamma)d$ ,  $d(d, n)^3\text{He}$ ,  $d(d, p)^3\text{H}$ , and  $d(p, \gamma)^3\text{He}$  reactions.

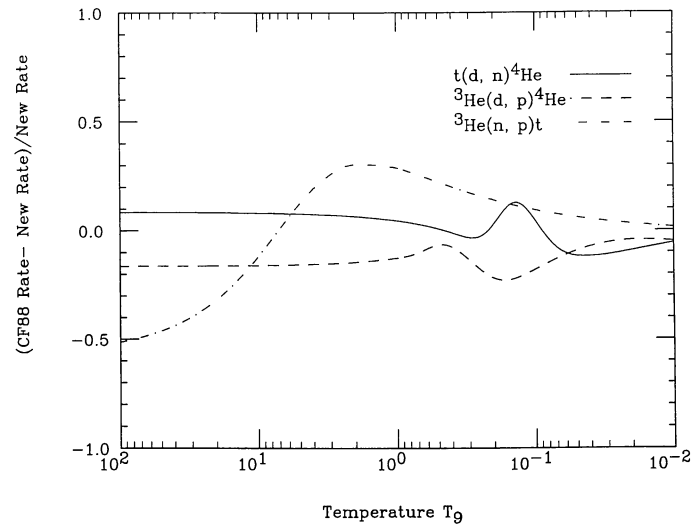


FIG. 25.—Fractional reaction rate difference for the  $t(d, n)^4\text{He}$ ,  ${}^3\text{He}(d, p){}^4\text{He}$ , and  ${}^3\text{He}(n, p)t$  reactions.

## 5. INFERRED PRIMORDIAL ABUNDANCES

### 5.1. Introduction

The above sections have described our effort to obtain the most precise prediction, with a conservative  $2\sigma$  uncertainty, of the abundances of D,  ${}^3\text{He}$ ,  ${}^4\text{He}$ , and  ${}^7\text{Li}$  as a function of the SBBN free parameter  $\eta$ . The comparison of these abundance predictions with the primordial abundances inferred from present observations determines the constraint on  $\eta$  that we seek. In this section, we summarize the observational data on light-element abundances, and determine conservative limits on inferred primordial abundances. In doing so, we assume the universality of abundances inferred from observations which are (necessarily) limited in range. The observations are within the solar system (meteoric and solar wind) for deuterium and  ${}^3\text{He}$ , within the galaxy (metal-deficient halo stars) for lithium, and extragalactic (nearby H II regions and dwarf galaxies, distance

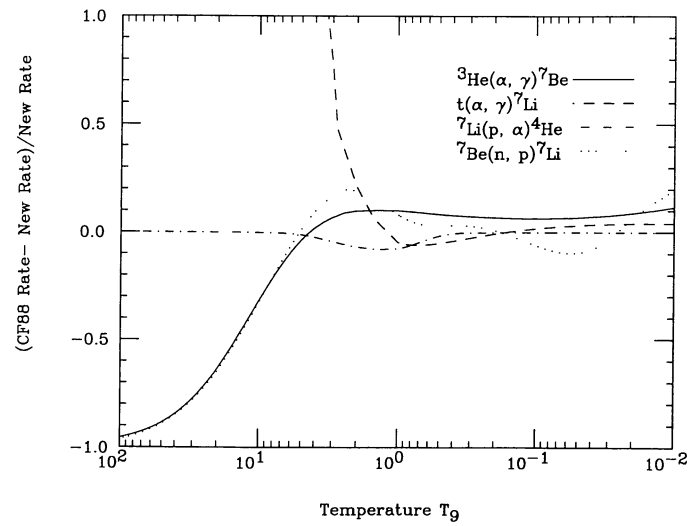


FIG. 26.—Fractional reaction rate difference for the  ${}^3\text{He}(\alpha, \gamma){}^7\text{Be}$ ,  $t(\alpha, \gamma){}^7\text{Li}$ ,  ${}^7\text{Li}(\alpha, \gamma){}^4\text{He}$ , and  ${}^7\text{Be}(\alpha, \gamma){}^8\text{Be}$  reactions.

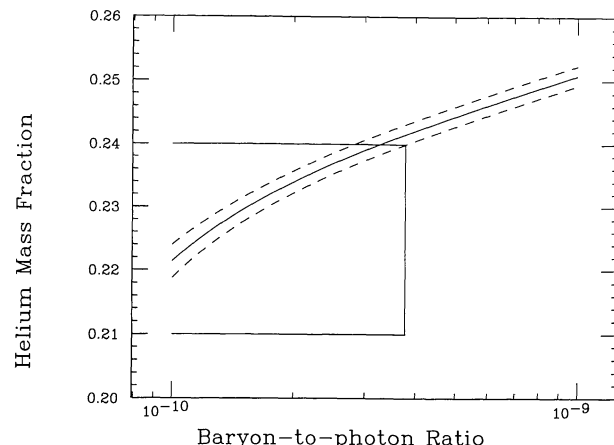


FIG. 27a

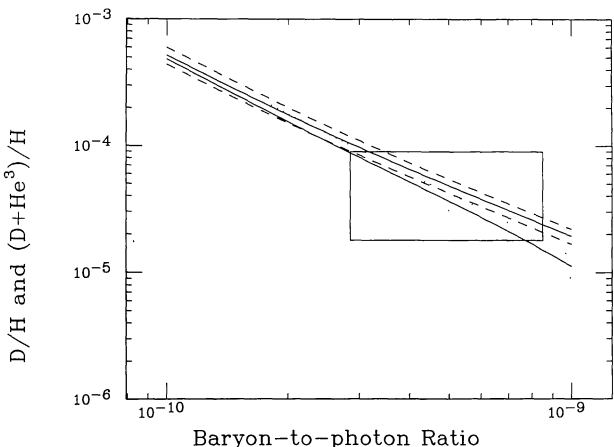


FIG. 27b

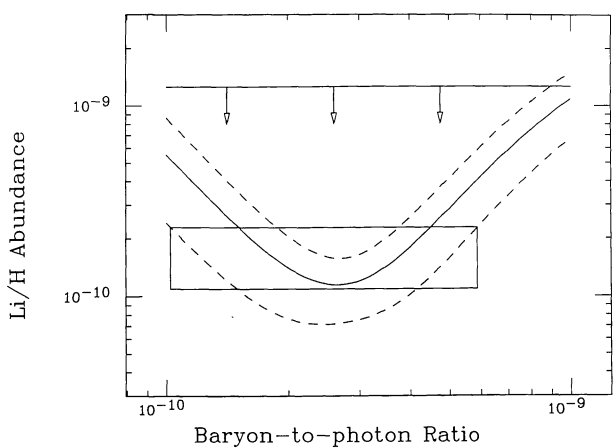


FIG. 27c

FIG. 27.—Light-element abundance vs. baryon-photon ratio  $\eta$  for (a)  $^4\text{He}$  mass fraction, (b) D/H and  $(\text{D} + ^3\text{He})/\text{H}$ , and (c)  $^7\text{Li}/\text{H}$ . The boxes indicate observationally acceptable regions for  $\eta$ ; the horizontal lines give upper and lower bounds to the deduced primordial abundances; the vertical lines show the resulting bounds on  $\eta$ . The dashed curves show the  $2\sigma$  abundance limits. The top horizontal line in plot(c) is the observational upper bound from Population I stars.

$\lesssim 100$  Mpc) for  $^4\text{He}$ . We must assume that these observed abundances represent those of the entire universe to draw conclusions concerning standard model parameters such as constraints on  $\eta$  or  $\Omega_b$ .

There are enough observational uncertainties to warrant a very cautious approach in setting abundance limits. Our goal is to obtain conservative estimates rather than best values. Even though the uncertainties placed on our inferred light-element abundance ranges do not have the same quantitative significance as the uncertainties of our numerical determinations of the abundance yields, they will allow us to obtain a robust limit on  $\eta$  and  $\Omega_b$ .

### 5.2. Primordial Deuterium

With a binding energy of 2.22 MeV, deuterium is the most fragile of the primordial isotopes: it is rapidly destroyed in

TABLE 4  
EFFECTS OF NEW NUCLEAR REACTION RATES

Reaction	D	$^3\text{He}$	$^4\text{He}$	$^7\text{Li}$
$\eta_{10} = 1.0$				
p(n, $\gamma$ )d .....	-5.42	1.26	0.47	-7.07
d(p, $\gamma$ ) $^3\text{He}$ .....	0.35	-0.62	0.00	-0.13
d(d, n) $^3\text{He}$ .....	2.50	3.28	-0.20	0.94
d(d, p)t .....	-1.01	-1.93	-0.10	2.14
$^3\text{He}(n, p)t$ .....	0.06	8.73	0.00	-0.61
t(d, n) $^4\text{He}$ .....	0.03	0.37	0.00	-1.39
$^3\text{He}(d, p)^4\text{He}$ .....	-0.06	-1.70	0.00	-0.44
$^3\text{He}(\alpha, \gamma)^7\text{Be}$ .....	0.00	0.00	0.00	-0.15
t( $\alpha, \gamma$ ) $^7\text{Li}$ .....	-0.01	0.00	0.00	3.52
$^7\text{Be}(n, p)^7\text{Li}$ .....	0.00	0.00	0.00	0.01
$^7\text{Li}(p, \alpha)^4\text{He}$ .....	0.01	0.00	0.00	-0.61
All reactions .....	-3.35	9.07	0.15	-3.94
$\eta_{10} = 3.0$				
p(n, $\gamma$ )d .....	-3.10	2.21	0.08	11.36
d(p, $\gamma$ ) $^3\text{He}$ .....	2.07	-3.30	0.00	-3.46
d(d, n) $^3\text{He}$ .....	6.32	0.71	-0.18	-5.17
d(d, p)t .....	1.17	0.89	-0.10	0.42
$^3\text{He}(n, p)t$ .....	-0.28	7.54	0.00	5.21
t(d, n) $^4\text{He}$ .....	0.03	0.10	0.00	-0.93
$^3\text{He}(d, p)^4\text{He}$ .....	-0.29	-4.29	0.00	-2.68
$^3\text{He}(\alpha, \gamma)^7\text{Be}$ .....	0.00	0.00	0.00	-4.47
t( $\alpha, \gamma$ ) $^7\text{Li}$ .....	0.00	0.00	0.00	0.87
$^7\text{Be}(n, p)^7\text{Li}$ .....	0.00	0.00	0.00	1.73
$^7\text{Li}(p, \alpha)^4\text{He}$ .....	-0.01	-0.01	0.00	-0.04
All reactions .....	6.31	2.78	-0.22	-0.81
$\eta_{10} = 6.0$				
p(n, $\gamma$ )d .....	-1.59	1.37	0.03	11.05
d(p, $\gamma$ ) $^3\text{He}$ .....	5.62	-5.74	0.00	-9.24
d(d, n) $^3\text{He}$ .....	8.67	-0.41	-0.17	-12.04
d(d, p)t .....	2.42	1.72	-0.11	-2.04
$^3\text{He}(n, p)t$ .....	-0.79	4.42	0.00	7.59
t(d, n) $^4\text{He}$ .....	0.01	0.03	0.00	-0.12
$^3\text{He}(d, p)^4\text{He}$ .....	-0.40	-5.89	0.00	-5.35
$^3\text{He}(\alpha, \gamma)^7\text{Be}$ .....	0.00	0.00	0.00	-7.59
t( $\alpha, \gamma$ ) $^7\text{Li}$ .....	0.00	0.00	0.00	0.04
$^7\text{Be}(n, p)^7\text{Li}$ .....	0.00	0.00	0.00	2.02
$^7\text{Li}(p, \alpha)^4\text{He}$ .....	0.00	0.00	0.00	0.00
All reactions .....	15.06	-5.36	-0.27	-18.22

stellar interiors, and it is therefore assumed that all primordial deuterium present in the initial stellar environment is destroyed. Although models of deuterium production in other astrophysical sites have been proposed (e.g., Ozernoi & Chernomordik 1976), none have obtained wide acceptance; the main arguments against post-big bang production of deuterium are outlined in Epstein, Lattimer, & Schramm (1976). Future observations of the D/H ratio as a function of radial distance from the Galactic center should help resolve this issue (Pasachoff & Vidal-Madjar 1989).

Given that significant quantities of deuterium can only be produced during primordial nucleosynthesis, detection of deuterium provides important evidence in favor of the big bang model. Because deuterium can only undergo a net destruction following the epoch of nucleosynthesis, the presently inferred abundance can only be used to place stringent *lower* limits on the primordial deuterium abundance  $D_p$ . Since the predicted deuterium abundance decreases rapidly as  $\eta$  increases in the SBBN model, an inferred lower limit to the deuterium abundance serves to bound  $\eta$  from above.

Deuterium was first observed extraterrestrially in the form of  $\text{CH}_3\text{D}$  in the Jovian atmosphere (Beer et al. 1972), as DCN in Galactic molecular clouds (Jefferts, Penzias, & Wilson 1973), and as HD and D I (Lyman series) in diffuse clouds (Spitzer et al. 1973; Rogerson & York 1973). Subsequently, observations of atomic deuterium Lyman absorption lines from the Copernicus satellite have provided extensive data on the interstellar D/H ratio up to distances of  $\sim 1$  kpc. Interpretation of these data was not, however, straightforward, principally due to the presence of several interstellar clouds in the different lines of sight; and a wide range of D/H was deduced, ranging from the pre-solar value of  $2 \times 10^{-5}$  to values as low as  $5 \times 10^{-6}$  (Boesgaard & Steigman 1985). Informative histories of deuterium observations can be found in Pagel (1987) and Pasachoff & Vidal-Madjar (1989).

Given the range of D/H observed in the interstellar medium, it is difficult to directly determine a lower limit to the primordial deuterium abundance; similarly, a determination of the upper limit to  $D_p$  is plagued by uncertainties arising from chemical evolution effects. The ratio of the primordial abundance of deuterium to that observed today could be anywhere between 1 and 50; see Pagel (1982), Delbourgo-Salvador et al. (1985), Pagel (1986), Larson (1986), and Audouze (1987). Because of the intrinsic uncertainties involved, we will forgo dealing directly with the deuterium abundance in our analysis, choosing instead to derive a lower limit on D from considerations of D +  $^3\text{He}$  (in § 5.4).

It has recently been suggested that the primordial deuterium abundance may be more directly probed in the relatively unprocessed matter of the Lyman- $\alpha$  forest clouds seen in QSO spectra. Although such a determination is fraught with experimental difficulty, there is hope that the next generation of detectors and telescopes will overcome these difficulties (Webb et al. 1991).

### 5.3. Primordial $^3\text{He}$

$^3\text{He}$  is known to be present in the solar wind from metal foils placed on the lunar surface, and from spectroscopic observations of solar flares. It is also observed in the interstellar me-

dium in H II regions at distances of  $\sim 20$  kpc from the Galactic center via the hyperfine transition of  $^3\text{He}^+$  at  $\lambda = 3.46$  cm (Rood et al. 1984; Bania, Rood, & Wilson 1987). The corrections involved in the analysis of this data limit its accuracy, but typical values for  $^3\text{He}/\text{H}$  are in the range  $2 \times 10^{-5}$ – $8 \times 10^{-5}$  (Bania et al. 1987).

As with deuterium, the abundance of primordial  $^3\text{He}$  cannot be directly determined from observations because of stellar processing: low-mass stars tend to produce  $^3\text{He}$ , while massive stars tend to destroy  $^3\text{He}$  (Schatzman 1987). Thus we turn to an analysis of D +  $^3\text{He}$  to reduce some of the uncertainties caused by stellar evolution.

### 5.4. Primordial D + $^3\text{He}$

As discussed above, our ignorance of the details of chemical evolution effects prevents a direct determination of primordial D and  $^3\text{He}$ . However, the pre-solar D abundance can be adopted as a *lower* limit to the primordial D abundance: the pre-solar D abundance should be larger than the present D abundance because of  $d(p, \gamma)^3\text{He}$  reactions and should not be larger than the primordial value in the absence of any post-big bang D production.

The pre-solar abundance of D and  $^3\text{He}$  can be determined from analysis of the carbonaceous chondrites (CC), which are believed to closely represent the primitive solar system matter out of which the Sun formed. On the other hand, the gas-rich meteorites (GRM) and the solar wind experiments provide data on the present abundance of the two isotopes. If indeed the  $^3\text{He}$  abundance as determined from the CC samples is adopted as the pre-solar value of  $^3\text{He}$ , and the  $^3\text{He}$  as determined from the GRM/solar wind samples is adopted as the combined pre-solar abundance of D *plus*  $^3\text{He}$ , then the pre-solar D-value can be determined as a difference of the two abundances (Black 1971; Geiss & Reeves 1972).

From their study of the available data set compiled in Pagel (1987), Walker et al. (1991) arrive at the following  $2\sigma$  ranges:

$$1.8 \leq 10^5 y_2 < 3.3 \quad (31a)$$

$$1.3 \leq 10^5 y_3 < 1.8 \quad (31b)$$

$$3.3 \leq 10^5 y_{23} < 4.9 , \quad (31c)$$

where  $y$  represents the number ratio relative to hydrogen and the subscripts 2, 3, and 23 represent the pre-solar values D,  $^3\text{He}$ , and D +  $^3\text{He}$ , respectively. A lower limit to the primordial D abundance of  $D_p \geq 1.8 \times 10^{-5}$  ( $2\sigma$ ) can therefore be adopted.

An upper limit to the primordial D abundance is more problematic and model dependent; there is no *a priori* determination of the amount of D destruction prior to formation of the pre-solar nebula. Since D is mainly destroyed via  $d(p, \gamma)^3\text{He}$ , some difficulties can be overcome by considering the total sum of D +  $^3\text{He}$ . There still remains, however, the problem of  $^3\text{He}$  production and destruction in stars. The uncertainty implicit in this process can be conveniently expressed by introducing the “survival fraction”  $g_3$ , which is the fraction of primordial  $^3\text{He}$  that survives stellar astration. In a simple one-cycle ap-

proximation we have

$$y_{23p} \leq y_{23} + (g_3^{-1} - 1)y_3, \quad (32)$$

where  $y_{23p}$  is the primordial abundance of D +  $^3\text{He}$ . On the assumption that  $g_3 \geq 0.25$  (Yang et al. 1984; Delbourgo-Salvador et al. 1985; Dearborn, Schramm, & Steigman 1986) we have  $y_{23p} \leq 9 \times 10^{-5}$ . Clearly this number is dependent on the approximations and assumptions of the chemical evolution model adopted (e.g., Walker et al. 1991), particularly on the initial mass function. Because of the inherent uncertainties of Galactic chemical evolution, we are skeptical as to the usefulness of more sophisticated models in this instance; we will therefore adopt the limit of  $y_{23p} \leq 9 \times 10^{-5}$  while being aware of its dependence on chemical evolution.

### 5.5. Primordial $^4\text{He}$

$^4\text{He}$  is very abundant in the universe, making up approximately one quarter of the baryonic mass. Estimates of the  $^4\text{He}$  abundance can therefore come from a variety of different sources: optical and radio emission lines from Galactic nebula, optical absorption lines in stars, atmospheric scale heights in the major planets, solar oscillation studies, and the effect of the helium abundance on stellar evolution and stellar photometry. A tabulation of the primordial  $^4\text{He}$  mass fraction,  $Y_p$ , inferred from these studies is given by Pagel (1987), who notes that these determinations of  $Y_p$  suffer from significant uncertainties, astration effects in particular, and are somewhat limited in their usefulness.

The most reliable determination of  $Y_p$ , it is believed, comes from the analysis of emission lines in metal-poor extragalactic H II regions and dwarf galaxies, where helium can be observed via the recombination of  $\text{He}^+$ . To trace the production of  $^4\text{He}$  by chemical evolution, the helium abundance is plotted as a function of metallicity and linearly extrapolated to zero metallicity. The value of the  $^4\text{He}$  mass fraction thus obtained is assumed equal to  $Y_p$ . Caution is required, however, in the use of high-metallicity sources such as the Sun and Orion in such extrapolations: it is not at all obvious why the  $^4\text{He}$  abundance in these objects should be given equal statistical weight as the lower-metallicity data points.

The existing H II data useful for determination of  $Y_p$  has been recently tabulated by Pagel (1991), who restricts the data set to H II regions with less than 0.25 solar metallicity. Pagel's analysis of his data set leads to the result  $Y_p = 0.225 \pm 0.005$  ( $1\sigma$ ) with oxygen as the metallicity tracer and  $Y_p = 0.229 \pm 0.004$  ( $1\sigma$ ) with nitrogen as the tracer. The question of the most appropriate metallicity tracer has been well discussed in the literature (Pagel, Terlevich, & Melnick 1986; Steigman, Gallagher, & Schramm 1989; Fuller et al. 1991). Walker et al. (1991) have recently reanalyzed a slightly extended version of the data set used in Pagel (1991) and arrive at similar conclusions. Further restricting the data set of low-metallicity objects, Fuller et al. used the 14 lowest-metallicity objects in the Pagel (1991) data set, and determined  $Y_p = 0.220 \pm 0.007$  ( $1\sigma$ ) using nitrogen as the tracer. They concluded that  $Y_p = 0.22 \pm 0.01$  was a more reasonable assessment of the primordial helium abundance.

We emphasize that the uncertainties on  $Y_p$  quoted above are purely statistical; it is not inconceivable that systematic errors

may be larger. Possible sources of such errors are collisional excitation, contribution of neutral helium, interstellar reddening, uncertainty of the ionizing UV-flux, and grain depletion. Davidson & Kinman (1985) review these types of error sources and conclude they could contribute as much as  $\pm 0.01$  to the uncertainty of  $Y_p$ . Pagel (1991) estimates the maximum systematic uncertainty to be somewhat lower, namely  $\pm 0.005$  ( $1\sigma$ ). There is the additional possibility that some site in the early galaxy produces significant quantities of  $^4\text{He}$  but very little metals; first generation massive Population II stars (Bond, Arnett, & Carr 1984) are most often discussed in this regard. Such a systematic source of error, implying even lower values of  $Y_p$ , would be very difficult to rule out completely.

A quantitative estimate of the systematic errors in a primordial  $^4\text{He}$  abundance determination is difficult to assess. We will adopt  $0.21 \leq Y_p \leq 0.24$  as a cautious and reasonable assessment. This range covers the lower limit estimated by Fuller et al. (1991) and is bounded by the  $2\sigma$  upper limit as determined by Pagel (1991) on the basis of his analysis of the data and his expectation of the systematic errors.

The upper limit to  $Y_p$  has very important implications: as we discuss later, an upper limit of  $Y_p \lesssim 0.23$ , as possibly indicated by the work of Fuller et al. (1991), would be inconsistent with SBBN. We will determine the lowest value of  $Y_p$  which can be made consistent with the inferred primordial abundances of the other isotopes given the abundance and nuclear reaction rate uncertainties. We note that the lower limit on  $Y_p$  plays no role in constraining  $\eta$ .

### 5.6. Primordial Lithium

Of all the primordial isotopes, the problem of inferring from the available data the primordial abundance of  $^7\text{Li}$  remains the most difficult and controversial. The principal reason for this difficulty is the large spread in the Li abundances observed in stars of different effective temperatures, ages, masses and compositions. Stellar modelers have spent a great deal of effort to fully understand the numerous trends uncovered by the observers. Although great progress has been made through these efforts, difficulties still persist, and some would argue that definitive conclusions based on the current data cannot yet be drawn.

There are two widely discussed scenarios concerning the Li abundance data. The first is to interpret the general increase in the extremes of the Li abundance data for higher metallicities as the gradual enrichment of Li in the galaxy from different nucleosynthesis processes. At the low values of  $[\text{Fe}/\text{H}] [= \log(\text{Fe}/\text{H})_* - \log(\text{Fe}/\text{H})_\odot]$  characteristic of Population II stars, no significant enrichment or depletion of Li has occurred, and the observed abundance is thought to closely resemble the pristine primordial abundance. The alternative scenario is that significant amounts ( $\sim$ Population I levels) of Li is produced during the big bang, and only very small amounts are produced during the history of the Galaxy. In this viewpoint, the low Li abundance seen in the Population II stars is a consequence of depletion mechanisms in these older stars and can therefore place no firm upper limit on the primordial Li. In fact, since astration of Li in stars is assumed to be important, even the high solar system value could be representative of the primordial value. The possibility remains, of course, for a combination of both scenarios.

Spurred by the ever-increasing accumulation of high quality spectra of metal-poor Population II stars and by new and improved stellar model calculations, an increasing number of researchers have argued for the correctness of the first of the above scenarios. We will first discuss the arguments in favor of this position.

### 5.6.1. Lithium in Population II Stars

The pioneering observations of Li abundances in Population II stars were carried out by Spite & Spite (1982). Their results have since been confirmed by several other extensive surveys (Spite, Maillard, & Spite 1984; Hobbs & Duncan 1987; Rebolo, Beckman, & Molaro 1988). When selective criteria are applied so as to include only the oldest and most extreme halo stars and to exclude those which have evolved off the main sequence, an unambiguous trend emerges in a plot of lithium abundance versus effective temperature [ $N(\text{Li})$  vs.  $T_{\text{eff}}$ ]. At low  $T_{\text{eff}}$  ( $\lesssim 5500$  K), the Li abundance decreases with decreasing  $T_{\text{eff}}$ ; at higher  $T_{\text{eff}}$  (5500–6300 K), there is a uniform plateau, with very little scatter, of constant Li abundance  $[\text{Li}] \sim 2.1$ , using the notation  $[\text{Li}] = 12 + \log (\text{Li}/\text{H})$ . Deliyannis, Demarque, & Kawaler (1990) have ascribed the decrease of Li at cooler temperatures to pre-main-sequence burning. The Li in the stars which make up the narrow uniform plateau, however, could not have been significantly affected by standard pre-main-sequence burning, and the Li abundances there are taken as representative of the primordial Li value.

In their detailed study of this issue, Deliyannis et al. (1990) surveyed the available data base and selected 35 stars as extreme halo stars to be used in their analysis. The selection criteria adopted was  $[\text{Fe}/\text{H}] \leq -1.3$  (low metallicity) and  $V_{\text{LSR}} \geq 160$  km s $^{-1}$  (high velocity with respect to the local standard of rest). This set of halo stars contains the oldest stars of our galaxy to within 1–5 Gyr. Their high space velocities imply the sampling of a large fraction of the protogalaxy. In the uniform plateau region, the data base contained 24 stars and 39 determinations of the Li abundance (some of the same stars were observed by the different groups). The minimal scatter of the Li abundances in this group of observations is quite remarkable: all of the data points are within a width of 0.34 in  $[\text{Li}]$  (30 are within 0.20), even though the star's metallicities cover over an order of magnitude in range ( $-2.7 \leq [\text{Fe}/\text{H}] \leq -1.3$ ). A naive averaging of the Li abundances within the plateau gives  $[\text{Li}] = 2.08 \pm 0.09$  (2  $\sigma$ ); a similar result is obtained from a weighted mean in Walker et al. 1991. When coupled with the low uncertainty ( $\pm 0.1$ –0.2) in each of the Li observations, this implies that there is no intrinsic dispersion in the data within this accuracy (however, see the discussion in § 5.6.2); dispersion in the data apparently only appears for  $[\text{Fe}/\text{H}] \gtrsim -1.5$ . This evidence suggests that the Li abundance observed in the plateau stars show no effects of intrinsic stellar processing and therefore closely represents the primordial abundance.

In a more sophisticated analysis, Deliyannis et al. (1990) constructed a series of Li isochrones for the parameter range  $10 \leq \text{stellar age} \leq 20$  Gyr,  $1.1 \leq \alpha \leq 1.5$  (ratio of mixing length to pressure scale height), and  $0.0001 \leq Z \leq 0.001$ ; the isochrones were then compared with their selected plateau stars using a  $\chi^2$  fitting procedure. By adopting a conservative

error on each of the observed abundance determinations of 0.2 and 0.4 for the plateau and cool stars, respectively, they derive a primordial Li value of

$$[\text{Li}]_p = 2.17^{+0.04}_{-0.13} (2 \sigma). \quad (33)$$

Since this value accounts for any small-scale depletion that can occur in the plateau stars, it is a much better estimate than a simple statistical mean of the plateau star abundances. In addition, Deliyannis et al. obtained acceptable  $\chi^2$  fits to the available data when microscopic diffusion (e.g., gravitational settling) was included into their standard stellar evolution codes. This resulted in some additional, albeit small, depletion of the primordial Li, altering the range for the primordial Li abundance to

$$[\text{Li}]_p = 2.31^{+0.05}_{-0.17} (2 \sigma). \quad (34)$$

The degree of diffusion is, however, very sensitive to uncertain physics (e.g., opacity). Additional studies by Deliyannis & Demarque (1991a) have suggested that the above range may be an overestimate of the Li depletion due to diffusion processes; see also Proffitt & Michaud (1991) and Chaboyer et al. (1992). Since depletion by microscopic diffusion represents a possible source of systematic error, and since we prefer here not to overinterpret the data, we will err on the side of caution and adopt the full range (using eqs. [33] and [34])  $2.04 \leq [\text{Li}]_p \leq 2.36$  (2  $\sigma$ ) as our primordial Li value from Population II halo stars.

We close this section by mentioning a few of the concerns regarding analyses of the Population II data. As noted above, the shape of the  $N(\text{Li})$ – $T_{\text{eff}}$  relation in the Population II main-sequence (MS) stars can be attributed to standard pre-MS burning (Deliyannis et al. 1990). The Deliyannis et al. (1990) models, however, *do not* require any additional (beyond standard model convection) mixing mechanisms on the pre-MS in order to fit the data, contradicting the earlier results of D'Antona & Mazzitelli (1984). Deliyannis et al. (1990) suggest that this discrepancy may be traced to the approximations used by D'Antona and Mazzitelli in their linear interpolations of opacities and equation of state. Another point of controversy concerns the metallicity dependence of the  $N(\text{Li})$ – $T_{\text{eff}}$  relation. D'Antona (1991) argues that observations imply a *unique*  $N(\text{Li})$ – $T_{\text{eff}}$  curve for metallicities differing by a factor greater than 2; the conclusion that the  $N(\text{Li})$ – $T_{\text{eff}}$  relation possess no metallicity dependence would be in contradiction to standard pre-MS evolution. D'Antona (1991) therefore suggests that an accurate understanding of the  $N(\text{Li})$ – $T_{\text{eff}}$  for Population II stars may still be lacking. Deliyannis & Demarque (1991b) challenge this, finding that Li depletion is indeed a function of metallicity, but that this result is still consistent with the available data. Keeping these problems in mind, we will adopt the 2  $\sigma$  primordial Li range  $2.04 \leq [\text{Li}]_p \leq 2.36$  for our present study.

Finally, we note that recent observations of two extreme Population II stars may indicate that the primordial  $[\text{Li}]$  value may be even lower than 2.0. The observations of G186–26 with  $[\text{Fe}/\text{H}] = -2.9$  (Hobbs, Welty, & Thorburn 1991; Beers, Deliyannis, & Ryan 1993) and of CS 22876–32 with  $[\text{Fe}/\text{H}] = -4.3$  (Molaro 1992) indicate *no* evidence for lithium

above background, setting upper limits of  $[Li] \lesssim 1.23$  and 1.8, respectively. Further observations of the most metal-poor stars ( $[Fe/H] < -3$ , tabulated in Beers, Preston, & Shectman 1993) are clearly necessary to determine whether these Li values are unique or truly representative of the primordial abundance (see also Thorburn 1992).

### 5.6.2. Lithium in Population I Stars

We will now consider the alternative hypothesis in which the primordial Li is approximately given by a Population I level and the low Li abundance seen in the Population II stars is a consequence of depletion mechanisms in these older stars. As we will discuss in § 6, this scenario may not allow for a range of  $\eta$  consistent with the other isotopic abundances.

The uncertainties regarding the interpretation of the Population I Li data are even more unclear than that for Population II Li data. The large spread in observations of the Population I Li abundance possibly indicates the operation of numerous depletion mechanisms which must be understood. For a Population I star of given mass, the opacity (a function of  $Z$ ) is the main factor controlling pre-MS Li burning. Larger values of opacity result in longer convective phases and consequently larger timescales for Li depletion. As discussed above, models of pre-MS depletion for halo stars have been constructed which can apparently account for the Population II data. However, similar models for Population I stars have not been able to adequately reproduce the  $N(Li) - T_{\text{eff}}$  relations observed in young open clusters. For example, at a given low value of  $T_{\text{eff}}$  in the Hyades, Li depletion is observed to be larger than predicted (Proffitt & Michaud 1989). One oft-discussed solution involves additional mixing at the pre-MS phase (D'Antona & Mazzitelli 1984; Vandenberg & Poll 1989); a second solution suggests larger opacities (e.g., Swenson, Stringfellow, & Faulkner 1990). Both these effects result in larger Li depletions. We caution, however, that both solutions overdeplete Li in younger clusters such as the Pleiades and alpha Per, and cannot account for the spread in abundances observed in these clusters.

There is the additional complication of the so called "Boesgaard Gap": Li depletion factors of 10–100 observed in a narrow range of  $T_{\text{eff}}$  at  $\sim 6700$  K (Boesgaard & Tripicco 1986; Boesgaard & Budge 1988) with the amount of Li depletion possibly correlated with the age of the stellar system. There have been numerous long timescale depletion mechanisms, beyond that of pre-MS depletion, proposed to explain this drop in Li: meridional circulation (Charbonneau & Michaud 1991), turbulent mixing induced by rotation (Vauclair 1988; Pinsonneault, Kawaler, & Demarque 1990; Charbonnel 1991), gravitational settling and other microscopic diffusion mechanisms (Michaud 1986; Proffitt & Michaud 1989), mass loss (Schramm, Steigman, & Dearborn 1990), and internal gravity waves (Lopez & Spruit 1991; Schatzman 1991).

Even though there is a large spread in the Population I Li abundance, possibly indicative of many depletion mechanisms, the maximum observed Li abundances in these stars seems to be approximately an order of magnitude larger than the Population II plateau value. The solar system value is  $[Li] \approx 3.3$ , although the actual solar value is approximately a factor of 100–200 smaller, probably as a consequence of rotational mixing (Pinsonneault et al. 1989). As alluded to earlier,

the alternative to the primordial Population II plateau interpretation is that the maximum Population I values are in fact more indicative of the primordial value, and that one or more astration mechanisms have reduced the Li abundance in some of the Population I stars and by a factor of  $\sim 10$  in all of the old Population II stars. The most widely discussed depletion mechanisms in this context are those associated with rotational breaking and the subsequent chemical mixing (Pinsonneault et al. 1990). The inclusion of rotation, however, magnifies the uncertainties in the input physics.

Pinsonneault et al. (1992) have carried out a detailed study the effects of rotation on the depletion factors of Population II stars, showing they can account for an essentially uniform depletion of the halo plateau stars by approximately one order of magnitude. The small dispersion in the plateau caused by the rotational depletion is extremely difficult to detect; however, by analyzing the available data in the color-equivalent width plane (which removes many of the uncertainties associated with transformation to the  $T_{\text{eff}}$ -abundance plane), Deliyannis & Pinsonneault (1993) claim the existence of a small dispersion of  $\sim 10\%$ . Such a dispersion is in fact consistent with the rotational depletion hypothesis. In addition, rotational depletion predicts that there should be the rare plateau star with a Li abundance well above the mean plateau value, corresponding to one with an unusually low initial angular momentum. Deliyannis & Pinsonneault (1993) argue that if interstellar reddening is taken into account, one of the plateau stars (BD  $23^{\circ} 3912$ ) does in fact possess a Li abundance a factor of  $\sim 50\%$  above the mean plateau abundance. If their interpretation of BD  $23^{\circ} 3912$  and of the intrinsic dispersion within halo plateau stars is supported by further research, it would support the conclusion that the present abundance of Li in the Population II plateau stars may *not* represent the primordial value. This possibility is of major concern: a primordial value near  $[Li]_p = 3.1$ , consistent the rotational depletion study of Pinsonneault et al. (1992), would *not* allow for a range of  $\eta$  consistent with the other isotopic abundances.

A complete understanding of the Galactic chemical evolution of Li still eludes us. We note that chemical evolution models exist for both the galactic enrichment hypothesis (e.g., Deliyannis 1990; D'Antona & Matteucci 1991) and for the galactic astration hypothesis (e.g., Mathews, Alcock, & Fuller 1990). These latter models adopted an initial primordial Li abundance even higher than the Population I value, yet were still able to simultaneously account for the Population I, the Population II, and the current solar system values. This clearly illustrates our incomplete understanding of the Li depletion mechanisms in stars.

### 5.7. Summary of Primordial Abundances

Our conservative limits on the primordial abundances inferred from observations are summarized in Table 5. The deuterium limit is obtained from the pre-solar value; the  $D + ^3He$  limit from solar system values using a simple one-cycle processing model; the  $^7Li$  range from the observations in Population II metal-deficient stars in the Galactic halo; and the  $^4He$  range from extrapolations of observations in extragalactic H II regions and dwarf galaxies to zero metallicity. New observations and new models do not allow us to definitively say that the

Population II Li level is the primordial value; we have therefore added in Table 5 the Population I level consistent with recent rotational stellar models. We now can compare our inferred abundances with those predicted in § 4, which are plotted against  $\eta$  in Figure 27.

## 6. COMPARISON OF OBSERVED AND PREDICTED PRIMORDIAL ABUNDANCES

As mentioned above, when we compare theory with observation, we realize that the uncertainties placed on our inferred light-element abundance ranges do not have the same statistical significance as the uncertainties on our numerical determinations of the abundance yields. However, through the use of conservative abundance limits, together with the Monte Carlo results incorporating nuclear uncertainties, we can still delineate a permitted range of  $\eta$  with great confidence. This range is determined with the help of Figures 27a–27c and 28, where the abundance limits (*horizontal lines*) are shown with the abundance predictions (*solid curves*) and  $2\sigma$  uncertainties (*dashed lines*) as functions of  $\eta$ . Table 5 lists our abundance limits and the corresponding constraints on  $\eta$ , and Figure 28 shows the overlap of the constraints from D +  $^3\text{He}$ ,  $^4\text{He}$ , and  $^7\text{Li}$ . We see that this region of consistency of  $\eta$  is bounded *from below* by the lower limit inferred on D +  $^3\text{He}$ , and bounded *from above* by the upper limit inferred on  $^4\text{He}$ :

$$2.86 \leq \eta_{10} \leq 3.77 . \quad (35)$$

Our upper bound of 5.87 on  $\eta_{10}$  from  $^7\text{Li}$  is 47% higher than the analogous bound found in Walker et al. (1991) ( $\eta_{10} \leq 4.0$ ) because the new reaction rates produce  $\approx 20\%$  less  $^7\text{Li}$  at high  $\eta$  values (Table 4). From the discussions in §§ 5.5 and 5.6, it is clear that there is substantially less uncertainty in the primordial  $^4\text{He}$  abundance than in the primordial  $^7\text{Li}$  abundance;  $Y_p$  therefore gives a *more robust* upper limit on  $\eta$ . Furthermore, since observations of  $^4\text{He}$  are made over a much larger distance scale than those of  $^7\text{Li}$ , we have greater confidence in our assumption of universality of these new limits.

In order to convert our allowed range of  $2.86 \leq \eta_{10} \leq 3.77$  into limits on the present baryon density, we need the present temperature of microwave photons  $T_\gamma$ . The weighted mean of measurements of  $T_\gamma$  at wavelengths  $\geq 1 \text{ mm}$  is  $T_\gamma = 2.76 \pm 0.02$  ( $2\sigma$ ), using the results from COBE (Mather et al. 1990) and from De Amici et al. (1991), Gush, Halpern, & Wishnow (1990), Kaiser & Wright (1990), Kogut et al. (1990), and Meyer et al. (1990), as well as the measurements listed in Palazzi et al. (1990).

It is convenient to express the baryon mass density,  $\rho_b$ , in relation to the mass density which closes the universe, the criti-

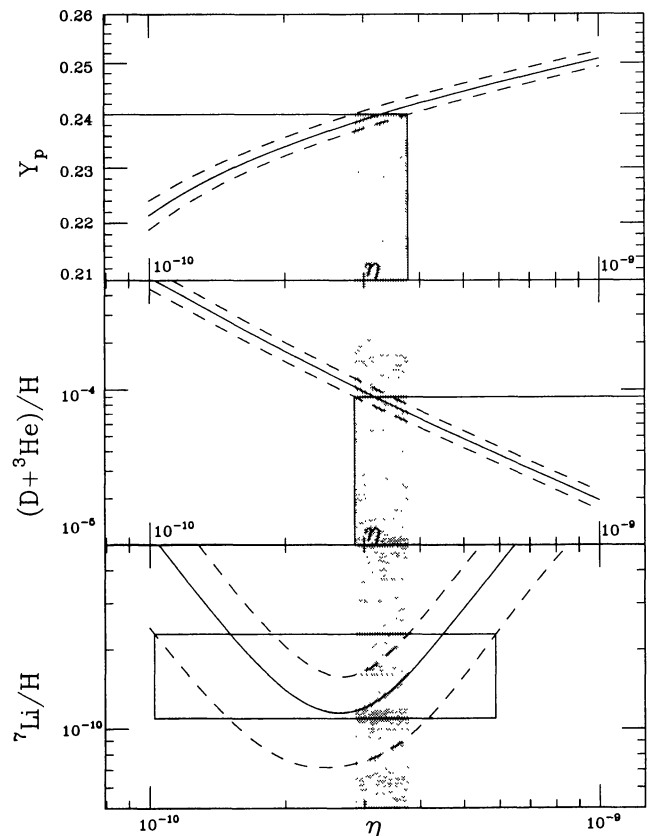


FIG. 28.—Plots from Fig. 27 arranged vertically. The shaded regions show the values of  $\eta$  for which there is concordance between computed abundances and observational constraints.

cal density

$$\rho_c = \frac{3H_o^2}{8\pi G}, \quad (36)$$

where  $H_o = 100 h \text{ km s}^{-1} \text{ Mpc}^{-1}$  is the present value of the Hubble parameter and  $h$  parameterizes its present observational uncertainty (reviewed in van den Bergh 1989 and Visvanathan 1990; see also Sandage & Tammann 1990). Defining  $\Omega_b$  as the ratio of baryonic to critical mass density ( $\Omega_b = \rho_b/\rho_c$ ), we can express  $\Omega_b$  as

$$\Omega_b h^2 = 3.73 \times 10^{-3} \left( \frac{T_\gamma}{2.75} \right)^3 \eta_{10} . \quad (37)$$

The allowed range of  $\eta$  (eq. [35]) can be used along with the

TABLE 5  
OBSERVATIONAL CONSTRAINTS

Element	Abundance Limit	Constraint
Deuterium .....	$D/H \geq 1.8 \times 10^{-5}$	$\eta_{10} \leq 8.52$
Deuterium and Helium-3 .....	$(D + {}^3\text{He})/H \leq 9.0 \times 10^{-5}$	$\eta_{10} \geq 2.86$
Helium-4 .....	$0.21 \leq Y_p \leq 0.24$	$0.63 \leq \eta_{10} \leq 3.77$
Lithium-7 .....	$1.1 \times 10^{-10} \leq {}^7\text{Li}/H \leq 2.3 \times 10^{-10}$ (Population II) ${}^7\text{Li}/H \leq 1.3 \times 10^{-9}$ (Population I)	$1.02 \leq \eta_{10} \leq 5.87$ $\eta_{10} \leq 11.3$

above value of  $T_\gamma$  to determine a permitted range in  $\Omega_b h^2$  of

$$0.011 \leq \Omega_b h^2 \leq 0.015 . \quad (38)$$

Allowing for the range  $0.4 \leq h \leq 1$ , this becomes

$$0.01 \leq \Omega_b \leq 0.09 . \quad (39)$$

The constraint on  $\Omega_b$  is shown as a function of  $h$  in Figure 29. The approximate factor of 2 uncertainty in the Hubble parameter introduces a factor of 4 uncertainty (the largest uncertainty) in the determination of  $\Omega_b$ . A more accurate assessment of  $H_o$ , one of the major goals of modern cosmology, would substantially reduce the total uncertainty in  $\Omega_b$ .

However cautious we may have been in assessing observational values, our assessments may still be disputed. Given the uncertainties implicit in the determination of the primordial  ${}^4\text{He}$  mass fraction as discussed in § 5.4, it is possible that our upper limit to  $Y_p$  is too restrictive. Because of the logarithmic dependence of  $Y_p$  on  $\eta$  (Fig. 28), the precise value of this upper limit is very important. For a bound  $Y_p < 0.247$ , for example, the constraint on  $\eta$  from  ${}^4\text{He}$  would be the same as that from the present upper limit from the  ${}^7\text{Li}$  abundance, and the resulting range for  $\Omega_b$  would become  $0.01 \leq \Omega_b \leq 0.14$ .

The lower limit on  $\Omega_b$  is less sensitive to changes in the  $D + {}^3\text{He}$  bound because  $(D + {}^3\text{He})/H$  has a steep  $\eta$  dependence (Fig. 28). For example, if the upper bound  $(D + {}^3\text{He})/H \leq 1 \times 10^{-4}$  is used, as in Walker et al., then the lower bound on  $\eta_{10}$  is decreased to 2.68 but there is no appreciable effect on the lower bound on  $\Omega_b$  of 0.01.

There are several immediate inferences that can be drawn from the limits given by equation (39). First, it is clear that the baryonic density falls far short of that required to close the universe ( $\Omega = 1$ ). Second, since the amount of luminous matter in the universe is constrained to be  $\Omega_{\text{lum}} \lesssim 0.007$  (e.g., Pagel 1990), baryonic dark matter is *required*. The argument for the necessity of non-baryonic dark matter is, however, less persuasive. There is tentative evidence that  $\Omega$  as inferred from galaxy

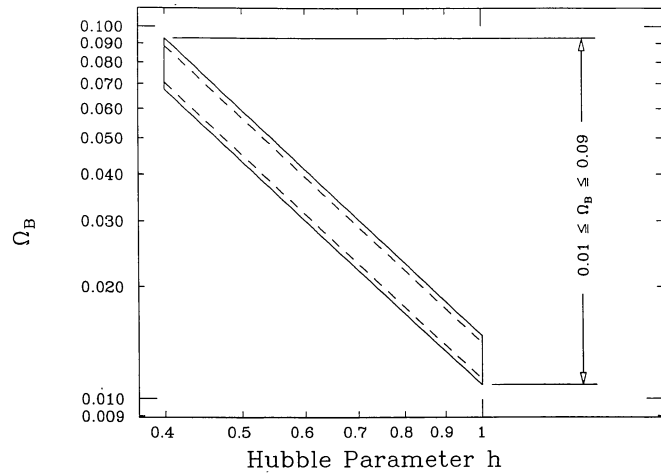


FIG. 29.—Constraint on baryon parameter  $\Omega_b$  vs. the Hubble expansion parameter. Acceptable values of  $\Omega_b$  are shown within the solid lines of the parallelogram. The dashed lines result from uncertainties in the CMB temperature.

cluster data, such as  $\Omega \approx 0.2$  for the Coma cluster (Hughes 1989), would seem to imply the existence of some form of non-baryonic matter. However, uncertainties could yet conspire to place this  $\Omega$  close to our inferred upper limit on  $\Omega_b$ . If larger values for  $\Omega$  become well established, such as those tentatively indicated by large-scale density fluctuations and peculiar velocities ( $\Omega = 0.75–1.15$ , assuming the bias factor for the *IRAS* galaxies is close to unity; Yahil 1990; Kaiser et al. 1991), then the constraints imposed by SBBN would imply the existence of some form of non-baryonic matter.

The present work shows that the SBBN model can consistently account for the primordial abundances of  $D$ ,  ${}^3\text{He}$ ,  ${}^4\text{He}$ , and  ${}^7\text{Li}$  as inferred from observation within a narrow range of the baryon-to-photon ratio  $\eta$ . However, there have been efforts to extend the range of  $\eta$  beyond that allowed for by SBBN by employing some new physics or by relaxing of some of the assumptions built into the SBBN model. Such nonstandard primordial nucleosynthesis models are reviewed in Malaney & Mathews (1993). Using only the inferred primordial abundances as our barometer, the present study shows that deviations from the SBBN model will be demanded if the range of  $Y_p$  is determined to be outside the range  $0.237 \leq Y_p \leq 0.247$ , assuming the constraints on  $D + {}^3\text{He}$  and  ${}^7\text{Li}$  remain firm. An upper limit of  $Y_p < 0.237$  would conflict with the  $D + {}^3\text{He}$  limit; although there is tentative evidence which suggest that the observed value of  $Y_p$  lies below 0.237 (Fuller et al. 1991), the systematic uncertainties do not yet allow for a strong case. Any firm conclusion, however, requiring modifications in either the abundance limits or SBBN, will most likely come from this quarter. We also note that increasing the  $(D + {}^3\text{He})/H$  bound to  $1.0 \times 10^{-4}$  would result in very little change in the  $Y_p$  value required for inconsistency (to 0.236).

New observations may also point to the inadequacy of SBBN. The recent measurements of Be and B in very metal-poor halo stars, by Ryan et al. (1992), Gilmore et al. (1991, 1992), and Duncan, Lambert, & Lemke (1992), cannot be explained in the SBBN model. These may be evidence for either a new production mechanism such as neutrino nucleosynthesis (Malaney 1992), a modified cosmic ray spallation process (Steigman & Walker 1992; Gilmore et al. 1992), or nonstandard (inhomogeneous) BBN models (where  $\Omega_b$  may be significantly enhanced—Boyd & Kajino 1989; Malaney & Fowler 1989). The observations of a Be and B “plateau” in these metal-poor stars would help to differentiate between the proposed scenarios.

Finally, as mentioned in § 5.6.2, a primordial Li abundance at the Population I level ( $[\text{Li}] \approx 3.1$ ), consistent with the rotational depletion study of Pinsoneault et al. (1992), would conflict with the limits from the other light isotopes. More specifically, if a lower limit of  $[\text{Li}] \geq 2.1$  ( $[\text{Li}/\text{H}] \geq 1.64 \times 10^{-10}$ ) can be set for the primordial Li abundance, then there will be a conflict with the limit from  ${}^4\text{He}$  ( $Y_p < 0.24$ ).

## 7. CONCLUSIONS

We have carried out a comprehensive experimental, computational, and observational analysis of the standard theory of primordial nucleosynthesis, employing the following: a detailed analysis of the rates and uncertainties of the most important nuclear reactions; a Monte Carlo analysis which gives ro-

bust  $2\sigma$  abundance predictions from the nuclear reaction rate uncertainties for the primordial isotopes D,  $^3\text{He}$ ,  $^4\text{He}$ , and  $^7\text{Li}$ ; a correction for errors in abundance predictions which arise from the numerical computation itself; and the most recent theoretical developments in obtaining inferred primordial abundances from observational data. The comparison of our numerical abundance predictions with those inferred from observations shows that consistent agreement can be achieved for all the light elements over a narrow range of the SBBN parameter  $\eta$ . This range is  $2.86 \leq \eta_{10} \leq 3.77$ , where the *lower* bound is from the primordial D +  $^3\text{He}$  abundance and the *upper* bound is from the primordial  $^4\text{He}$  abundance; this is in contrast to previous studies which used the less certain primordial  $^7\text{Li}$  abundance to bound  $\eta$  from above. The permitted range of  $\eta$  corresponds to a constraint on the baryon mass density parameter of  $0.01 \leq \Omega_b \leq 0.09$ . In determining this constraint on  $\Omega_b$ , we have assumed three relativistic neutrino species and the universality of the abundance observations used to infer primordial abundances.

It should be noted that the largest remaining uncertainty in the present constraint on  $\Omega_b$  (the uncertainty in the Hubble

parameter  $H_0$ ) lies outside the scope of this study. The uncertainty in the primordial abundances inferred from observational data account for the next largest uncertainty. In § 3, we discussed the key nuclear reactions for which a more accurate determination of the rates would be useful in further constraining  $\Omega_b$ . A firm determination that  $Y_p < 0.237$  will require either modification of the SBBN theory, or a re-interpretation of the D +  $^3\text{He}$  bound. It will be of wide-ranging interest, particularly with regard to non-baryonic dark matter or inhomogeneous models, to observe if the validity and consistency of SBBN theory remains intact.

The authors would like to thank Dick Azuma, Charles Barnes, Timothy Beers, Richard Boyd, Carl Brune, Constantine Deliyannis, Willy Fowler, Ralph Kavanagh, Lawrence Krauss, Peter Parker, Erich Ormand, Kenneth Sale, and Wallace Sargent for helpful discussions, and Michel Casse for pointing out typographical errors in the preprint version of Table 1. This work was supported by the NSF at Caltech under grants PHY88-17296 and PHY91-15574.

## REFERENCES

- Audouze, J. 1987, in IAU Symp. 124, Observational Cosmology, ed. A. Hewitt, G. Burbidge, & L. Z. Fang (Dordrecht: Reidel), 89
- Ajzenberg-Selove, F. 1988, Nucl. Phys., A, 490, 1
- Alfimenkov, V. P., et al. 1980, JINR, R3-80-394, Dubna
- . 1990, Soviet Phys.-JETP Lett., 52, 373
- Ageron, P., Mampe, W., Bates, J. C., & Pendlebury, J. M. 1986, Nucl. Instr. Meth., A249, 261
- Alexander, T. K., Ball, G. C., Lennard, W. N., Geissel, H., & Mak, H.-B. 1984, Nucl. Phys., A427, 526
- Altmeyer, T., Kolbe, E., Warmann, T., Langanke, K., & Assenbaum, H. J. 1988, Z. Phys., A330, 277
- Andrzejewski, J., Gledenov, Yu. M., Popov, Yu. P., Salatski, V. I., & Pshenichnyj, V. A. 1991, Z. Phys., A340, 105
- Anton, F., Paul, W., Mampe, W., Paul, L., & Paul, S. 1989, Nucl. Instr. Meth., A284, 101
- Argo, H. V., Taschek, R. F., Agnew, H. M., Hemmendinger, A., & Leland, W. T. 1952, Phys. Rev., 87, 612
- Arnold, W. R., Phillips, J. A., Sawyer, G. A., Stovall, E. J., Jr., & Tuck, J. L. 1954, Phys. Rev., 93, 483
- Assenbaum, H. J., Langanke, K., & Rolfs, C. 1987, Z. Phys., A327, 461
- Bailey, G. M., Griffiths, G. M., Olivo, M. A., & Helmer, R. L. 1970, Canadian J. Phys., 48, 3059
- Bahcall, N. A., & Fowler, W. A. 1969, ApJ, 157, 659
- Bania, T. M., Rood, R. T., & Wilson, T. L. 1987, ApJ, 323, 30
- Barker, F. C. 1972, ApJ, 173, 477
- Batchelor, R., Aves, R., & Skyrme, T. H. R. 1955, Rev. Sci. Instr., 26, 1037
- Baur, G., Bertulani, C. A., & Rebel, H. 1986, Nucl. Phys., A458, 1988
- Beaudet, G., & Reeves, H. 1984, A&A, 134, 240
- Beer, R., Farmer, C. B., Morton, R. H., Martonchik, J. V., & Barnes, T. G. 1972, Science, 175, 1360
- Beers, T. C., Deliyannis, C. P., & Ryan, S. 1993, in preparation
- Beers, T. C., Preston, G. W., Shectman, S. A. 1993, ApJ, in press
- Bethe, H. A., & Morrison, P. 1956, Elementary Nuclear Theory, 2nd ed. (NY: Wiley)
- Black, D. C. 1971, Nature Phys. Sci., 231, 1480
- Bluge, G., & Langanke, K. 1990, Phys. Rev., C41, 1191
- Bluge, G., Langanke, K., Reusch, H. G., & Rolfs, C. 1989, Z. Phys., A333, 219
- Boesgaard, A. M., & Budge, K. G. 1988, ApJ, 332, 410
- Boesgaard, A. M., & Steigman, G. 1985, ARA&A, 23, 319
- Boesgaard, A. M., & Tripicco, M. J. 1986, ApJ, 302, L49
- Bond, J. R., Arnett, W. D., & Carr, B. 1984, ApJ, 280, 825
- Bondarenko, L. N. 1982, KIAE 3666/2, Moscow, preprint
- Bondarenko, L. N., Kurguzov, V. V., Prokof'ev, Yu. A., Rogov, E. V., & Spivak, P. E. 1978, Soviet Phys.-JETP Lett., 28, 303
- Booth, D. L., Preston, G. R., & Shaw, P. F. D. 1956, Proc. Phys. Soc. Lond., A69, 265
- Borzakov, S. B., Malecki, H., Pikel'ner, L. B., Stempinski, M., & Sharapov, E. I. 1982, Soviet J. Nucl. Phys., 35, 307
- Bosman, M., Bol, A., Gilot, J. F., Leleux, P., Lipnik, P., & Macq, P. 1979, Phys. Lett., 82B, 212
- Boyd, R. N., & Kajino, T. 1989, ApJ, 336, L55
- Brettscher, E., & French, A. P. 1949, Phys. Rev., 75, 1154
- Brown, R. E., & Jarmie, N. 1990, Phys. Rev., C41, 1391
- Brown, R. E., Jarmie, N., & Hale, G. M. 1987, Phys. Rev., C35, 1999
- Brugger, R. M. 1957, Philips Petroleum Co., IDO Rep. No. 16373, 49
- Brune, C., Kavanagh, R. W., & Rolfs, C. R. 1992, private communication
- Burzynski, S., Czerski, K., Marcinkowski, A., & Zupranski, P. 1987, Nucl. Phys., A473, 179
- Byrne, J. 1982, Rep. Progr. Phys., 45, 115
- Byrne, J., et al. 1980, Phys. Lett., 92B, 274
- . 1990, Phys. Rev. Lett., 65, 289
- Caughlan, G. R., & Fowler, W. A. 1988, Atomic Data Nucl. Data, 40, 291
- Cervena, J., Havranek, V., Hnatowicz, V., Kvitek, J., Mastalka, A., & Vacik, J. 1989, Czech. J. Phys., B39, 1263
- Chaboyer, B., Deliyannis, C. P., Demarque, P., Pinsonneault, M. H., & Sarajedini, A. 1992, ApJ, 388, 372
- Charbonel, C. 1991, Mem. Soc. Astron. Ital., in press
- Charbonneau, P., & Michaud, G. 1991, ApJ, 370, 693
- Christensen, C. J., Nielsen, A., Bahesen, A., Brown, W. K., & Rustad, B. M. 1967, Phys. Lett., B26, 11
- . 1972, Phys. Rev., D5, 1628
- Christy, R. F., & Duck, I. 1961, Nucl. Phys., 24, 89
- Clayton, D. D. 1983, Principles of Stellar Evolution and Nucleosynthesis (Chicago: Univ. Chicago Press)
- Conner, J. P., Bonner, T. W., & Smith, J. R. 1952, Phys. Rev., 88, 468
- Coon, J. H. 1950, Phys. Rev., 80, 488
- Costello, D. G., Friesenhahn, S. J., & Lopez, W. M. 1970, Nucl. Sci. Engineering, 39, 409
- D'Angelo, N. 1959, Phys. Rev., 114, 285
- D'Antona, F. 1991, Osservatorio Astronomico Di Roma OAR/91/7, preprint
- D'Antona, F., & Matteucci, F. 1991, A&A, 248, 62
- D'Antona, F., & Mazzitelli, I. 1984, A&A, 138, 431
- Davidenko, V. A., Pogrebov, I. S., & Saukov, A. I. 1957, J. Nucl. Engineering, 2, 258

- Davidson, K., & Kinman, T. D. 1985, ApJS, 58, 321
- De Amici, G., Bersanelli, M., Kogut, A., Levin, S., Limon, M., & Smoot, G. F. 1991, ApJ, 381, 341
- Dearborn, D. S. P., Schramm, D. N., & Steigman, G. 1986, ApJ, 302, 35
- Delbourgo-Salvador, P., Gry, C., Malinie, G., & Audouze, J. 1985, A&A, 150, 53
- Deliyannis, C. P. 1990, Ph.D thesis, Yale Univ.
- Deliyannis, C. P., & Demarque, P. 1991a, ApJ, 370, L89
- . 1991b, ApJ, 379, 216
- Deliyannis, C. P., & Pinsonneault, M. H. 1993, ApJ, submitted
- Deliyannis, C. P., Demarque, P., & Kawaler, S. D. 1990, ApJS, 73, 21
- Dicus, D. A., Kolb, E. W., Gleeson, A. M., Sudarshan, E. C. G., Teplitz, V. L., & Turner, M. S. 1982, Phys. Rev., D26, 2694
- Dohner, J., Abele, H., Reichert, I., Borel, H., Dubbers, D., Freedman, S. J., & Last, J. 1989, Nucl. Instr. Meth., A284, 123
- Dubbers, D. 1991, Prog. Part. Nucl. Phys., 26, 173
- Duncan, D., Lambert, D., & Lemke, D. 1992, ApJ, 401, 584
- Engstler, S., Krauss, A., Langanke, K., Neldner, K., Rolfs, C., Schroder, U., & Somorjai, E. 1989, ATOMKI 1988 Ann. Rep., 39
- Engstler, S., Krauss, A., Neldner, Rolfs, C., Schroder, U., & Langanke, K. 1988, Phys. Lett., 202B, 179
- Epstein, R. I., Lattimer, J. M., & Schramm, D. N. 1976, Nature, 263, 198
- Esmailzadeh, R., Starkman, G. D., & Dimopoulos, S. 1991, ApJ, 378, 504
- Evans, R. D. 1955, The Atomic Nucleus (NY: McGraw-Hill)
- Feldman, G., Balbes, M. J., Kramer, L. H., Williams, J. Z., Weller, H. R., & Tilley, D. R. 1990, Phys. Rev., C42, R1167
- Fick, D., & Weiss, U. 1973, Z. Phys., 265, 87
- Fowler, W. A., Caughlan, G. R., & Zimmerman, B. A. 1967, ARA&A, 5, 525 (FCZI)
- . 1975, ARA&A, 13, 69 (FCZII)
- Freedman, S. 1990, Comm. Nucl. Part. Phys., 19, 209
- Fuller, G. M., Boyd, R. N., & Kalen, J. D. 1991, ApJ, 371, L11
- Ganeev, A. S., Govorov, A. M., Osetinskii, G. M., Rakivnenko, A. N., Sizov, I. V., & Siksin, V. S. 1957, Atomnaya Energiya Suppl., 5, 21
- Gazes, S. B., Mason, J. E., Roberts, R. B., & Teichmann, S. G. 1992, Phys. Rev. Lett., 68, 150
- Geiss, J., & Reeves, H. 1972, A&A, 18, 126
- Gibbons, J. H., & Macklin, R. L. 1959, Phys. Rev., 114, 571
- Gilmore, G., Gustafson, B., Edvardson, B., & Nissen, P. E. 1992, Nature, 357, 379
- Gilmore, G., Edvardson, B., & Nissen, P. 1991, ApJ, 378, 17
- Gledenov, Yu. M., et al. 1986, JINR Rapid Comm., 17–86, 36
- Griffiths, G. M., Lal, M., & Scarfe, C. D. 1963, Canadian J. Phys., 41, 724
- Griffiths, G. M., Larson, E. A., & Robertson, L. P. 1962, Canadian J. Phys., 40, 402
- Griffiths, G. M., Morrow, R. A., Riley, P. J., & Warren, J. B. 1961, Canadian J. Phys., 39, 1397
- Gush, H. P., Halpern, M., & Wishnow, E. H. 1990, Phys. Rev. Lett., 65, 537
- Hale, G. M., Dodder, D. C., Siciliano, E. R., & Wilson, W. B. 1991, ENDF/B-VI Evaluation, Material 125, Revision 1
- Hanna, R. C. 1955, Phil. Mag., 46, 381
- Harmon, J. F. 1989, Nucl. Instr. Meth., B40/41, 507
- Harris, M. J., Fowler, W. A., Caughlan, G. R., & Zimmerman, B. A. 1983, ARA&A, 21, 165
- Hikasa, K., et al. 1992, Phys. Rev. D, 45, S1
- Hill, J. C., Wohn, F. K., Schwellenbach, D. D., & Smith, A. R. 1991, Phys. Lett., B273, 371
- Hilgemeier, M., Becker, H. W., Rolfs, C., Trautvetter, H. P., & Hammer, J. W. 1988, Z. Phys., A329, 243
- Hobbs, L. M., & Duncan, D. K. 1987, ApJ, 317, 796
- Hobbs, L. M., Welty, D. E., & Thorburn, J. A. 1991, ApJ, 373, L47
- Horsley, A. 1966, Nucl. Data, A2, 243
- Howerton, R. J. 1959, Univ California Radiation Lab. Rep. No. 5226 (Berkeley, CA: Univ. California)
- Hughes, J. P. 1989, ApJ, 337, 21
- Hughes, D. J., & Schwartz, R. B. 1958, Brookhaven Natl. Lab. Rep. BNL 325, 2d ed.
- Jarmie, N., Brown, R. E., & Hardekopf, R. A. 1984, Phys. Rev., C29, 2031
- Jarmie, N., & Brown, R. E. 1985, Nucl. Instr. Meth., B10/11, 405
- Jarvis, R. G., & Roaf, D. 1953, Proc. R. Soc. Lond., A218, 432
- Jefferts, K. B., Penzias, A. A., & Wilson, R. W. 1973, ApJ, 179, L57
- Kaiser, N., Efstathiou, G., Ellis, R., Frenk, C., Lawrence, A., Rowan-Robinson, M., & Saunders, W. 1991, MNRAS, 252, 1
- Kaiser, M. E., & Wright, E. L. 1990, in IAU Symp. 139, Galactic and Extragalactic Background Radiation—Optical, Ultraviolet, and Infrared Components, ed. S. Bowyer & C. Lienert (Dordrecht: Kluwer), 390
- Kajino, T. 1986, Nucl. Phys. A, 460, 559
- Kajino, T., & Arima, A. 1984, Phys. Rev. Lett., 52, 739
- Kajino, T., Mathews, G. J., & Ikeda, K. 1989, Phys. Rev., C40, 525
- Kajino, T., Toki, H., & Austin, S. M. 1987, ApJ, 319, 531
- Kawano, L. H. 1988, FERMILAB-PUB-88/34-A, preprint
- . 1992, FERMILAB-PUB-92/04-A, preprint
- Kharitonov, A. G., et al. 1989, Nucl. Instr. Meth., A284, 98
- Kim, H. J., Milner, W. T., & McGowan, F. K. 1966, Nucl. Data Tables, A1, 203
- Koehler, P. E., et al. 1988, Phys. Rev., C37, 915
- Kogut, A., Bensadoun, M., De Amici, G., Levin, S., Smoot, G. F., & Witebsky, C. 1990, ApJ, 355, 102
- Kolb, E. W., & Turner, M. S. 1990, The Early Universe (NY: Addison-Wesley)
- Kossakowski, R., Liaud, P., Azuelos, G., Grivot, P., & Schreckenbach, K. 1989, Nucl. Phys., A503, 473
- Kosvintsev, Yu. Yu., Kushnir, Yu. A., Morozov, V. I., & Terekhov, G. I. 1980, Soviet Phys.—JETP Lett., 31, 236
- Kosvintsev, Yu. Yu., Morozov, V. I., & Terekhov, G. I. 1986, Soviet Phys.—JETP Lett., 44, 571
- Kosvintsev, Yu. Yu., Morozov, V. I., Terekhov, G. I., Panin, Yu. N., Rogov, E. V., & Fomin, A. I. 1987, Proc. 1st Internat. Conf. on Neutron Physics, Vol. 1 (Kiev), ed. 231
- Krauss, A., Becker, H. W., Trautvetter, H. P., Rolfs, C., & Brand, K. 1987, Nucl. Phys., A465, 150
- Krauss, L. M. 1991, Yale Univ. YCTP-P4-91, preprint
- Krauss, L. M., & Romanelli, P. 1990, ApJ, 358, 47
- Krawinkel, H., et al. 1982, Z. Phys., A304, 307
- Kugler, K.-J., Paul, W., & Trinks, U. 1978, Phys. Lett., B72, 422
- Langanke, K. 1986, Nucl. Phys. A, 457, 351
- Langanke, K., & Rolfs, C. 1989, Mod. Phys. Lett., A4, 2101
- Larson, R. B. 1986, MNRAS, 218, 409
- Last, J., Arnold, J., Dohner, J., Dubbers, D., & Freedman, S. J. 1988, Phys. Rev. Lett., 60, 995
- Liskien, H., & Paulsen, A. 1973, Nucl. Data Tables, 11, 569
- Lopez, R. J. G., & Spruit, H. C. 1991, ApJ, 377, 268
- Macklin, R. L., & Gibbons, J. H. 1958, Phys. Rev., 109, 105
- . 1965, EANDC-50-S, Vol. 1, Paper 13
- Malaney, R. A. 1992, ApJ, 398, L45
- Malaney, R. A., & Fowler, W. A. 1989, ApJ, 345, L5
- Malaney, R. A., & Mathews, G. J. 1993, Phys. Rep., in press
- Mampe, W., Ageron, P., Bates, C., Pendlebury, J. M., & Steyerl, A. 1989, Nucl. Instr. Meth., A284, 111; 1989, Phys. Rev. Lett., 63, 593
- Mason, J. E., Gazes, S. B., Roberts, R. B., & Teichmann, S. G. 1992, Phys. Rev., C45, 2870
- Mather, J. C., et al. 1990, ApJ, 354, L37
- Mathews, G. J., Alcock, C. R., & Fuller, G. M. 1990, ApJ, 349, 449
- McNeill, K. G., & Keyser, G. M. 1951, Phys. Rev., 81, 602
- Mertelmeier, T., & Hofmann, H. M. 1986, Nucl. Phys. A459, 387
- Meyer, D. M., Roth, K. C., & Hawkins, I. 1990, in IAU Symp. 139, Galactic and Extragalactic Background Radiation—Optical, Ultraviolet, and Infrared Components, ed. S. Bowyer & C. Lienert (Dordrecht: Kluwer), 392
- Michaud, G. 1986, ApJ, 302, 650
- Molaro, P. 1992, Mem. Soc. Astron. Ital., 62, 17
- Moller, W., & Besenbacher, F. 1980, Nucl. Instr. Meth., 168, 111
- Morozov, V. I. 1989, Nucl. Instr. Meth., 284, 108
- Mughabghab, S. F., Divadeenam, M., & Holden, N. E. 1981, Neutron Cross Sections, Vol. 1, Neutron Resonance Parameters and Thermal Cross Sections, Part A,  $Z = 1\text{--}60$ , (NY: Academic Press)
- Nagatani, K., Dwarakanath, M. R., & Ashery, D. 1969, Nucl. Phys., A128, 325
- Olive, K. A., Schramm, D. N., Steigman, G., Turner, M. S., & Yang, J. 1981, ApJ, 246, 557
- Olive, K. A., Schramm, D. N., Steigman, G., & Walker, T. P. 1990, Phys. Lett., B236, 454

- Osborne, J. L., Barnes, C. A., Kavanagh, R. W., Kremer, R. M., Mathews, G. J., Zyskind, J. L., Parker, P. D., & Howard, A. J. 1982, *Phys. Rev. Lett.*, 48, 1664; 1984, *Nucl. Phys.*, A419, 115
- Ozernoi, L. M., & Chernomordik, V. V. 1976, *Soviet Astron.*, 19, 693
- Pagel, B. E. J. 1982, *Phil. Trans. R. Soc. Lond.* A307, 19
- . 1986, in *Inner Space/Outer Space*, ed. E. W. Kolb, M. S. Turner, D. Lindley, K. Olive, & D. Seckel (Chicago: Univ. Chicago Press), 72
- . 1987, in *A Unified View of the Macro and Micro Cosmos*, ed. A. De Rujula, D. V. Nanopoulos, & P. A. Shaver (Singapore: World Scientific), 399
- . 1990, in *Baryonic Dark Matter*, ed. D. Lynden-Bell & G. Gilmore (Dordrecht: Kluwer), 237
- . 1991, *Phys. Scripta*, T36, 7
- Pagel, B. E. J., Terlevich, R. J., & Melnick, J. 1986, *PASP*, 98, 1005
- Palazzi, E., Mandolesi, N., Crane, P., Kutner, M. L., Blades, J. C., & Hegyi, D. J. 1990, *ApJ*, 357, 14
- Parker, P. D., & Kavanagh, R. W. 1963, *Phys. Rev.*, 131, 2578
- Pasachoff, J. M., & Vidal-Madjar, A. 1989, *Comm. Astrophys.*, 14, 61
- Paul, W., Anton, F., Paul, L., Paul, S., & Mampe, W. 1989, *Z. Phys.*, C45, 25
- Paul, W., & Trinks, U. 1978, *Fundamental Physics with Reactor Neutrons and Neutrinos*, Inst. Phys. Conf. Ser. No. 42, ed. T. von Egidy (Bristol: The Institute of Physics), 18; 1978, *La Recherche*, 9, 1008
- Perry, J. E., & Bame, S. J. 1955, *Phys. Rev.*, 99, 1368
- Pinsonneault, M. H., Deliyannis, C. P., & Demarque, P. 1992, *ApJS*, 78, 179
- Pinsonneault, M. H., Kawaler, S. D., & Demarque, P. 1992, *ApJS*, 74, 179
- Pinsonneault, M. H., Kawaler, S. D., Sofia, S., & Demarque, P. 1989, *ApJ*, 338, 424
- Preston, G., Shaw, P. F. D., & Young, S. A. 1954, *Proc. R. Soc. Lond.*, A226, 206
- Proffitt, C. R., & Michaud, G. 1989, *ApJ*, 346, 976
- . 1991, *ApJ*, 371, 584
- Raimann, G., et al. 1990, *Phys. Lett.*, 249B, 191
- Rebolo, R., Beckman, J. E., & Molaro, P. 1988, *A&A*, 192, 192
- Riley, S. P., & Irvine, J. M. 1991, *J. Phys.*, G17, 35
- Robertson, R. G. H., Dyer, P., Bowles, T. J., Brown, R. E., Jarmie, N., Maggiore, C. J., & Austin, S. M. 1983, *Phys. Rev.*, C27, 11
- Robson, J. M. 1950a, *Phys. Rev.*, 77, 747
- . 1950b, *Phys. Rev.*, 78, 311
- . 1951, *Phys. Rev.*, 83, 349
- Rolfs, C. 1992, private communication
- Rolfs, C., & Kavanagh, R. W. 1986, *Nucl. Phys.*, A455, 179
- Rolfs, C., & Rodney, W. S. 1988, *Cauldrons in the Cosmos* (Chicago: Univ. Chicago Press)
- Rood, R. T., Bania, T. M., & Wilson, T. L. 1984, *ApJ*, 280, 629
- Rogerson, J. B., & York, D. G. 1973, *ApJ*, 186, L95
- Ryan, S. G., Norris, J. E., Bessel, M. S., & Deliyannis, C. P. 1992, *ApJ*, 388, 184
- Sandage, A., & Tammann, G. A. 1990, *ApJ*, 365, 1
- Schatzman, E. 1987, *A&A*, 172, 1
- Schatzman, E. 1991, *Mem. Soc. Astron. Ital.*, in press
- Schramm, D. N., & Kawano, L. 1989, *Nucl. Instr. Meth.*, A284, 84
- Schramm, D. N., Steigman, G., & Dearborn, D. S. P. 1990, *ApJ*, 359, L55
- Schreckenbach, K., Azuelos, G., Grivot, P., Kossakowski, R., & Liaud, P. 1989, *Nucl. Instr. Meth.*, A284, 120
- Schroder, U., Engstler, S., Krauss, A., Neldner, K., Rolfs, C., Somorjai, E., & Langanke, K. 1989, *Nucl. Instr. Meth.*, B40/41, 466
- Schroder, U., Redder, A., Rolfs, C., Azuma, R. E., Buchmann, L., Campbell, C., King, J. D., & Donoghue, T. R. 1987, *Phys. Lett.*, 142B, 55
- Shapiro, F. L. 1958, *Soviet Phys.-JETP Lett.*, 7, 1132
- Snell, A. H., & Miller, L. C. 1948, *Phys. Rev.*, 74, 1217
- Snell, A. H., Pleasanton, F., & McCord, R. V. 1950, *Phys. Rev.*, 78, 310
- Sosnovski, A. N., Spivak, P. E., Prokof'ev, Yu. A., Kutikov, I. E., & Dobrinin, Yu. P. 1959, *Nucl. Phys.*, 10, 395
- Spinka, H., Tombrello, T., & Winkler, H. 1971, *Nucl. Phys. A*, 164, 1
- Spite, M., & Spite, F. 1982, *A&A*, 115, 357
- Spite, M., Maillard, J. P., & Spite, F. 1982, *A&A*, 141, 56
- Spitzer, L., Drake, J. F., Jenkins, E. B., Morton, D. C., Rogerson, J. B., & York, D. G. 1973, *ApJ*, 181, L116
- Spivak, P. E. 1988, *Soviet Phys.-JETP Lett.*, 67, 1735
- Spivak, P. E., Sosnovski, A. N., Prokof'ev, Yu. A., & Sukolov, V. S. 1956, *Proc. Internat. Conf. on Peaceful Uses of Atomic Energy* (Geneva), Vol. 2 (NY: United Nations), 33
- Stehn, J. R., Goldberg, M. D., Magurno, B. A., & Wiener-Chasman, R. 1964, *BNL-325*, 2d ed., Suppl. 2, Vol. 1
- Steigman, G., Gallagher, J., & Schramm, D. N. 1989, *Comm. Astrophys.*, 14, 97
- Steigman, G., & Walker, T. P. 1992, *ApJ*, 385, L13
- Swenson, F. J., Stringfellow, G. S., & Faulkner, J. 1990, *ApJ*, 348, L33
- Theus, R. B., McGarry, W. I., & Beach, L. A. 1966, *Nucl. Phys.*, 80, 273
- Thorburn, J. A. 1992, *ApJ*, 399, L83
- Utsunomiya, H., et al. 1990, *Phys. Rev. Lett.*, 65, 847
- van den Bergh, S. 1989, *A&AR*, 1, 111
- VandenBerg, D. A., & Poll, H. E. 1989, *AJ*, 98, 1451
- Vauclair, S. 1988, *ApJ*, 335, 971
- Visvanathan, N. 1990, *Australian J. Phys.*, 43, 189
- Volk, H., Krawinkel, H., Santo, R., & Wallek, L. 1983, *Z. Phys.*, A310, 91
- Wagoner, R. V. 1969, *ApJS*, 18, 247
- Walker, T. P., Steigman, G., Schramm, D. N., Olive, K. A., & Kang, H.-S. 1991, *ApJ*, 376, 51
- Webb, J. K., Carswell, R. F., Irwin, M. J., & Penston, M. V. 1991, Royal Greenwich Obs. (RGO) 91-0045, preprint
- Weinberg, S. 1972, *Gravitation and Cosmology* (NY: Wiley)
- Williams, R. D., & Koonin, S. E. 1981, *Phys. Rev. C*, 23, 2773
- Yahil, A. 1990, in *Particle Astrophysics*, ed. J.-M. Alimi, A. Blanchard, A. Bouquet, F. M. de Volnay, & J. T. T. Van (Gif-sur-Yvette: Editions Frontières), 483
- Yang, J., Turner, M. S., Steigman, G., Schramm, D. N., & Olive, K. A. 1984, *ApJ*, 281, 493
- Zhichang, L., Jingang, Y., & Xunliang, D. 1977, *Chin. J. Sci. Technique Atomic Energy*, 3, 229